

MolFM: A Multimodal Molecular Foundation Model

Yizhen Luo¹, Kai Yang¹, Massimo Hong^{1,2}, Xingyi Liu¹, Zaiqing Nie^{1,*}

¹Institute of AI Industry Research (AIR), Tsinghua University

²Department of Computer Science and Technology, Tsinghua University

{yz-luo22,hongcd21}@mails.tsinghua.edu.cn

liuxingyi99@gmail.com {yangkai,zaiqing}@air.tsinghua.edu.cn

Abstract

Molecular knowledge resides within three different modalities of information sources: molecular structures, biomedical documents, and knowledge bases. Effective incorporation of molecular knowledge from these modalities holds paramount significance in facilitating biomedical research. However, existing multimodal molecular foundation models exhibit limitations in capturing intricate connections between molecular structures and texts, and more importantly, none of them attempt to leverage a wealth of molecular expertise derived from knowledge graphs. In this study, we introduce MolFM, a multimodal molecular foundation model designed to facilitate joint representation learning from molecular structures, biomedical texts, and knowledge graphs. We propose cross-modal attention between atoms of molecular structures, neighbors of molecule entities and semantically related texts to facilitate cross-modal comprehension. We provide theoretical analysis that our cross-modal pre-training captures local and global molecular knowledge by minimizing the distance in the feature space between different modalities of the same molecule, as well as molecules sharing similar structures or functions. MolFM achieves state-of-the-art performance on various downstream tasks. On cross-modal retrieval, MolFM outperforms existing models with 12.13% and 5.04% absolute gains under the zero-shot and fine-tuning settings, respectively. Furthermore, qualitative analysis showcases MolFM’s implicit ability to provide grounding from molecular substructures and knowledge graphs. Code and models are available on <https://github.com/BioFM/OpenBioMed>.

1 Introduction

The understanding of molecular properties and functions is of great significance to broad biomedical applications. Molecular knowledge resides within three multimodal information sources, namely molecular structures, biomedical documents and knowledge bases. Recent advances in Vision-and-Language Pre-training (VLP) [1–7] have sparked the emergence of pre-trained multimodal molecular foundation models that jointly learn molecular representations from structures and semantically-related texts. These approaches can be categorized as follows: (1) Generative models, exemplified by KV-PLM [8] and MolT5 [9], which treat the SMILES string of molecules and texts in a unified model with an auto-encoding framework. (2) Contrastive models, including MoMu [10] and MoleculeSTM [11], which conduct contrastive learning with the structural and textual representations of molecules.

Despite their promising advancements, existing multimodal molecular foundation models suffer from the following key limitations: (1) They fail to fully exploit and fuse the available structural and text information. Generative models primarily rely on 1D SMILES strings to capture structural characteristics and therefore lack the ability to interpret complex topological and spatial properties like macrocycles [8, 12]. Contrastive models, on the other hand, tend to overlook the intricate

*Corresponding author

connections between text snippets and substructures of molecules. (2) Existing models predominantly focus on local-level domain knowledge from individual molecules and neglect crucial global-level domain knowledge from knowledge bases. In fact, it has been widely accepted that incorporating global-level knowledge including relationships among molecules, target ligands, diseases and other biomedical entities could greatly facilitate biomedical research [13–15].

In this work, we propose MolFM, a multimodal molecular foundation model, to address the aforementioned problems. We aim to conduct joint molecular representation learning that captures both the local knowledge between molecular structures and biomedical texts, as well as the global knowledge from knowledge bases. To accomplish this goal, we first encode 2D molecular graphs, biomedical texts and knowledge graphs independently with pre-trained single-modal encoders. Then, we introduce a multimodal encoder to holistically fuse the features with cross-modal attention between atoms of the molecular structure, neighbors within the knowledge graph and tokens in the textual description. We incorporate structure-text contrastive (STC), cross-modal matching (CMM), masked language model (MLM) and knowledge graph embedding (KGE) as pre-training objectives. More importantly, we provide theoretical justifications that our multimodal pre-training could be interpreted as minimizing the distance in the feature space between different modalities of the same molecule, as well as between molecules that share similar structures or functions.

We manifest the outstanding performance of MolFM on various downstream tasks. On cross-modal retrieval [16, 8, 10], MolFM achieves absolute gains of 12.13% and 5.04% under zero-shot and fine-tuning settings, respectively, compared to the state-of-the-art method MoMu [10]. On molecule captioning and text-based molecule generation [9], we show that MolFM generates more accurate molecules and text descriptions through quantitative and qualitative studies. On molecular property prediction [17], MolFM boosts the prediction performance by 1.55% absolute gain on average by incorporating multimodal data. We also provide visualization of cross-modal attention, which reveals MolFM’s potential to perform grounding based on molecular sub-structures and knowledge graphs.

Our contributions are summarized as follows: (1) We propose MolFM, a multimodal molecular foundation model designed to facilitate joint representation learning from molecular structures, biomedical texts, and knowledge graphs through fine-grained cross attention between different modalities. (2) We theoretically justify that our pre-training approach implicitly minimizes the distance in the feature space between different modalities of the same molecule, as well as between molecules with similar structures or functions. (3) We show the state-of-the-art performance of MolFM on various downstream tasks, thereby highlighting its efficacy and versatility.

2 Related works

Our work is connected to the following research topics:

Molecular foundation models. Due to insufficient supervised data in the biomedical domain, molecular foundation models that conduct pre-training on large-scale unsupervised molecules have been developed. Most existing works primarily focus on a single modality of molecules. One line of research aims to learn molecular knowledge from structural representations such as 1D SMILES strings [18, 19], 2D molecular graphs [20–23] or 3D geometry views [24–26]. Another line attempts to implicitly capture molecular expertise through comprehending biomedical literature [27–30].

More recently, several multimodal approaches [8–11] that jointly learn molecular representations from molecular structures and biomedical texts have been proposed. For example, KV-PLM [8] and MolT5 [9] treat SMILES strings and texts as two different languages and perform pre-training with auto-encoding objectives [31, 32]. MoMu [10] and MoleculeSTM [11] encode molecular graphs and texts with independent encoders and conduct cross-modal contrastive learning [3, 4]. Different from these models, MolFM connects molecular expertise from three modalities, namely structures, texts and knowledge graphs, enabling a more holistic understanding of molecules.

Knowledge-empowered deep learning for molecules. The incorporation of domain knowledge has shown significant efficacy in various molecule-related tasks, including drug-drug interaction prediction [33], drug-target binding affinity prediction [34, 35], and molecular property prediction [15]. However, there are only a few attempts in knowledge-enhanced molecular foundation models. Existing works include MoCL [36] that employs substructure perturbation knowledge and structural similarity knowledge to generate positive samples for contrastive learning. Similarly, KCL [37] augments 2D molecular graphs with the guidance of chemical element knowledge. In contrast,

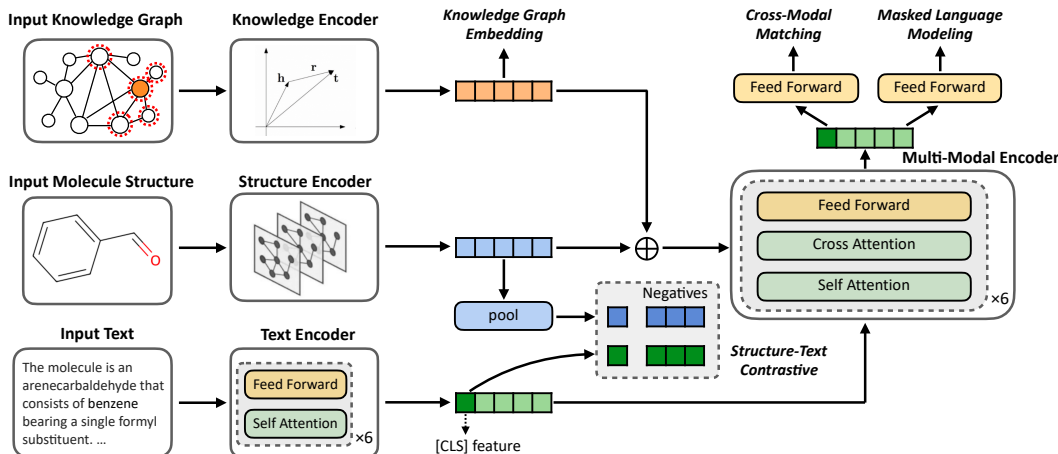


Figure 1: **Pre-training pipeline of MolFM.** We formulate the knowledge graph input for each molecule (dashed circle) as the corresponding entity (orange node) and its 1-hop neighbors. MolFM employs three independent single-modal encoders to convert multimodal inputs into feature vectors. Additionally, it comprises a multimodal encoder to integrate fine-grained connections between atoms, neighboring entities and textual tokens. We leverage structure-text contrastive learning to align the feature space between two modalities, cross-modal matching loss and masked language modeling loss to promote a holistic understanding of multimodal information, and a knowledge embedding loss as a regularization term.

MolFM treats knowledge graphs as an additional input modality instead of a tool to generate structural augmentations. Furthermore, MolFM focuses on capturing richer global knowledge of molecules, such as their relationships with other compounds, target ligands or diseases.

3 MolFM Pre-training

In this section, we start with a brief introduction to our model architecture (Sec. 3.1), followed by the multimodal pre-training objectives (Sec. 3.2). Then, we provide theoretical justifications for our approach from the perspective of deep metric learning (Sec. 3.3). Finally, we describe our pre-training dataset and knowledge graph (Sec. 3.4), as well as implementation details (Sec. 3.5).

3.1 Model architecture

The model architecture of MolFM is illustrated in Fig. 1. MolFM aims to learn a joint representation from molecular structure S , biomedical text T and knowledge graph input K . We formalize S as a 2D molecular graph $\mathcal{G} = (\mathcal{V}, \mathcal{E})$ where \mathcal{V} represents atoms and \mathcal{E} represents bonds, and T as a sequence of L tokens. We define the overall knowledge graph KG as a graph containing entities as nodes and relations as edges. KG is represented by a set of triplets $\{(h, r, t)\}$ where h and t are head and tail entities, and r is the relation type. Considering that biomedical texts often contain co-occurring mentions of entities related to the molecule [30], we formulate K as the corresponding molecular entity in KG and N randomly sampled entities from its one-hop neighbors. In this way, K comprises richer information from knowledge graphs to facilitate further multimodal pre-training.

MolFM utilizes three independent encoders pre-trained on single-modality data to encode inputs from different modalities. The molecular graph encoder employs a 5-layer GIN [38] initialized with the weights from GraphMVP [23] to obtain node representations h_{SA} for atoms and a graph representation h_{SM} for the entire molecule. The text encoder adopts a 6-layer transformer [39] initialized with the first 6 layers of KV-PLM [8] to generate token features h_T . The knowledge graph encoder implements a TransE [40] model, which has been trained on KG for 500 epochs, to compute knowledge features h_K for each entity in K .

Inspired by [5], we introduce a multimodal encoder composed of 6 transformer layers with cross attention at each layer. The multimodal encoder is initialized as the last 6 layers of KV-PLM. The cross attention module performs multimodal fusion using token features h_T as queries and the concatenation of atom features h_{SA} and neighbor features h_K as keys and values.

3.2 Pre-training objectives

Our pre-training procedure contains 4 objectives: structure-text contrastive loss (STC), cross-modal matching (CMM), masked language modeling (MLM) and knowledge graph embedding (KGE).

Structure-text contrastive loss aims to align the feature space of structure and text encoders and further facilitate multimodal understanding. We apply fully-connected layers and l_2 normalization to obtain structural representation z_S from h_{SM} and textual representation z_T from $h_T^{[cls]}$ (the textual feature of the $[CLS]$ token). Then, we optimize the following cross-modal contrastive loss [3]:

$$\mathcal{L}_{stc} = -\frac{1}{2} \left[\log \frac{\exp(s(z_S, z_T)/\tau)}{\sum_{S' \in B} \exp(s(z_{S'}, z_T)/\tau)} + \log \frac{\exp(s(z_S, z_T)/\tau)}{\sum_{T' \in B} \exp(s(z_S, z_{T'})/\tau)} \right], \quad (1)$$

where $s(\cdot, \cdot)$ refers to cosine similarity, B consists of molecular structures and texts within the same mini-batch, and τ is a temperature hyper-parameter.

Cross-modal matching loss aims to promote a deeper understanding of molecules by predicting whether the structure, text and knowledge graph data correspond to the same molecule. We randomly permute the multimodal inputs in the mini-batch to create negative samples. We obtain the representation of the $[CLS]$ token from our multimodal encoder \mathcal{M}_θ , and feed it into the predictor p_{cmm} composed of a fully-connected layer and softmax activation. CMM optimizes the following loss:

$$\mathcal{L}_{cmm} = \sum_{(\tilde{S}, \tilde{T}, \tilde{K}) \in \tilde{B}} H \left[y_{cmm}(\tilde{S}, \tilde{T}, \tilde{K}), p_{cmm}(\mathcal{M}_\theta(h_{\tilde{S}}, h_{\tilde{T}}, h_{\tilde{K}})) \right], \quad (2)$$

where \tilde{B} is the corrupted mini-batch with $y_{cmm}(\tilde{S}, \tilde{T}, \tilde{K})$ indicating whether the multimodal data from the mini-batch correspond to the same molecule. $H(\cdot, \cdot)$ denotes cross entropy.

Masked language modeling loss aims to predict the masked tokens using information from three modalities. We adopt the same masking strategy as BERT [31] to generate the masked text \hat{T} , and minimize the following objective:

$$\mathcal{L}_{mlm} = H[y_{mlm}(\hat{T}), p_{mlm}(\mathcal{M}_\theta(h_S, h_{\hat{T}}, h_K))], \quad (3)$$

where p_{mlm} predicts the probability for masked tokens, and $y_{mlm}(\hat{T})$ is the one-hot ground truth.

Knowledge graph embedding loss serves as a regularization term to prevent the knowledge graph representations from catastrophic forgetting [41]. We randomly sample a positive triplet (h, r, t) from KG for each entity h in K . Then we generate two negative triplets (h, r, \tilde{t}) and (\tilde{h}, r, t) by randomly sampling \tilde{t}, \tilde{h} from all entities and optimize the following max-margin loss:

$$\mathcal{L}_{kge} = \sum_{h \in K} \left[\max(0, d(h, r, t) - d(h, r, \tilde{t}) + \Delta) + \max(0, d(h, r, t) - d(\tilde{h}, r, t) + \Delta) \right], \quad (4)$$

where $d(h, r, t) = \|f(h) + g(r) - f(t)\|_2$, and Δ is a margin hyper-parameter. We use f and g to denote embedding functions for entities and relations of our TransE model.

MolFM pre-training optimizes the sum of the aforementioned objectives where $\mathbb{E}[\cdot]$ is expectation:

$$\mathcal{L} = \mathbb{E}_{(S, T, K)} [\mathcal{L}_{stc} + \mathcal{L}_{cmm} + \mathcal{L}_{mlm} + \mathcal{L}_{kge}]. \quad (5)$$

3.3 Theoretical justifications

The relationship between conventional multimodal pre-training objectives (STC and MLM) and mutual information maximization has been studied in previous works [42, 5]. In this section, we interpret CMM and KGE from the perspective of deep metric learning [43, 44] with a brief introduction to our major findings, and defer readers to Appendix A.4 for detailed proofs.

CMM learns a fine-grained metric between the multimodal representations of the same molecule. We show that \mathcal{L}_{cmm} in Eq. 2 satisfies the following:

$$\mathcal{L}_{cmm} \propto \sum_{(\tilde{S}, \tilde{T}, \tilde{K}) \in \tilde{B}} [-p_{cmm}(\mathcal{M}_\theta(h_S, h_T, h_K)) + p_{cmm}(\mathcal{M}_\theta(h_{\tilde{S}}, h_{\tilde{T}}, h_{\tilde{K}}))]. \quad (6)$$

Eq. 6 conceptualizes that the multimodal encoder and the CMM predictor compose a scoring function which assigns higher scores to matched structure-text-knowledge triplets and lower scores for unmatched triplets. Therefore, we conclude that CMM further aligns the feature space of three modalities and captures the intrinsic connections between multimodal features.

KGE minimizes the distance between molecules sharing similar structures and functions. We formulate the max-margin loss in Eq. 4 as a function of the positive triplet (h, r, t) . Then, we present two lemmas for structurally and functionally similar molecules in the following:

Lemma 1. *Let r_s be a **symmetric** relation indicating structural similarity. Assuming that structurally similar molecules h and t satisfies $(h, r_s, t) \in KG$ and $(t, r_s, h) \in KG$, the following holds:*

$$\mathcal{L}_{kge}(h, r_s, t) \propto 2\|f(h) - f(t)\| - \|f(h) - f(\tilde{t})\| - \|f(\tilde{h}) - f(t)\|. \quad (7)$$

Lemma 2. *Assuming that for functionally similar molecules h and t , there exists some entity o and relation r that satisfies $(h, r, o) \in KG$, $(t, r, o) \in KG$ **or** $(o, r, h) \in KG$, $(o, r, t) \in KG$. We use \mathcal{I} to denote the triplets between h, t and these intermediate entities o . The following holds:*

$$\|f(h) - f(t)\| \leq \alpha \mathbb{E}_{(e_1, r, e_2) \sim \mathcal{I}} [\mathcal{L}_{kge}(e_1, r, e_2)] + C, \quad (8)$$

where $\alpha \approx 1$ and $C \approx 0$ are constants.

Lemma 1 shows that \mathcal{L}_{kge} pulls close the entity embeddings of structurally similar molecules and pushes away dissimilar molecules. In Lemma 2 we hypothesize that functionally similar molecules tend to interact with the same entity (e.g. treats the same disease). Then, we show that the mean \mathcal{L}_{kge} over \mathcal{I} serves as an upper bound for the distance between functionally similar molecules. Hence, by combining CMM and KGE, we empower our multimodal encoder with local knowledge from molecular structures and texts, as well as global knowledge from knowledge graphs.

3.4 Pre-training dataset and knowledge graph

We follow the pre-training data in [10], which consists of 15K molecules from PubChem [45] and 37M paragraphs from S2ORC [46]. We construct our knowledge graph using public databases [47–49] and heuristics [36]. The knowledge graph contains a total of 49K entities and 3.2M relations. We present more details in Appendix C.

3.5 Implementation details

The MolFM model comprises a molecular structure encoder with 1.8M parameters, a text encoder with 61.8M parameters, a knowledge encoder with 12.6M parameters, and a multi-modal encoder with 61.8M parameters. We pre-train MolFM for 300 epochs with a batch size of 128 on 4 NVIDIA A100 GPUs. We use the AdamW [50] optimizer with a weight decay of $1e^{-4}$. The learning rate is linearly warmed-up to $1e^{-4}$ in the first 2,000 iterations and then decreases to $1e^{-5}$ following a cosine annealing strategy. We set $N = 4$, $\tau = 0.1$ and $\Delta = 0.2$.

4 Downstream tasks

In this section, we present 4 downstream tasks and their fine-tuning strategy.

Cross-modal retrieval contains two sub-tasks, namely structure-to-text retrieval (S-T) and text-to-structure retrieval (T-S). We evaluate MolFM on PCdes [8] in both zero-shot and fine-tuning scenarios with the entire paragraph as text input. We report MRR (mean reversed rank) and Recall at 1/5/10. As depicted in Fig. 2a and Fig. 2b, we modify the re-ranking algorithm in [5] with an ensemble technique [16]. Specifically, we simultaneously optimize the fine-tuning objective and CMM loss in Eq. 2 during fine-tuning. For inference, we first retrieve the top- k candidates based on cosine similarity. Then, we calculate the CMM logits for these k candidates. Finally, we re-rank them by a linear combination of cosine similarities and CMM logits.

Molecule captioning involves generating descriptions based on molecular structures. We conduct experiments on the ChEBI-20 dataset [16] and follow the evaluation metrics in [9]. As shown in Fig. 2c, we apply a fully-connected layer to project the atom features h_{SA} and concatenate the results with outputs from the MolT5 [9] encoder. Then, we use the MolT5 decoder to generate the caption.

Text-based molecule generation refers to the task of generating the SMILES strings of molecules using textual descriptions as input. Once again, we utilize the ChEBI-20 dataset and evaluation

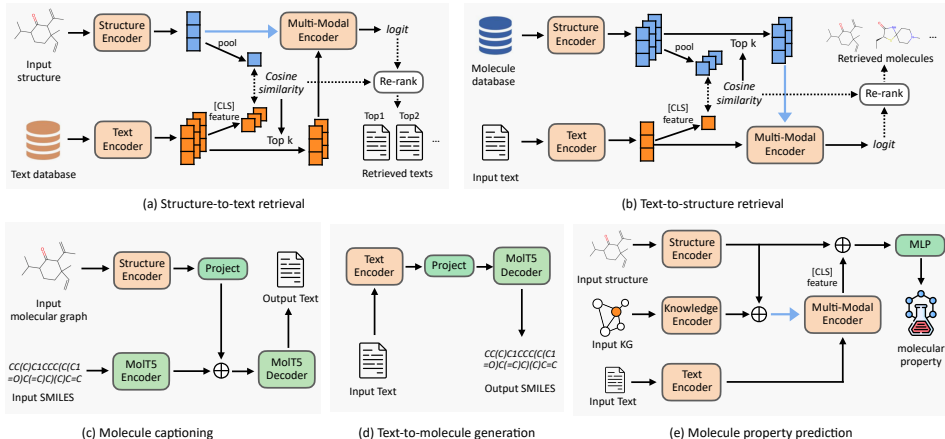


Figure 2: **Model architecture for downstream tasks.** For cross-modal retrieval, we re-rank top-k retrieved results with an ensemble of cosine similarity and CMM logit. For molecule captioning, we concatenate MolFM’s structure encoder outputs with MolT5 encoder outputs, and use the MolT5 decoder to generate texts. For text-to-molecule generation, we append a MolT5 decoder to generate SMILES strings. For molecular property prediction, we concatenate the output of structure encoder and multimodal encoder to fit the molecular property.

metrics in [9]. As illustrated in Fig. 2d, we pass the text features h_T through a fully-connected layer and feed them into the MolT5 decoder to generate SMILES strings.

Molecular property prediction is a vital task in AI-assisted drug discovery. We adopt MoleculeNet [17], a widely recognized benchmark encompassing 8 classification datasets whose prediction objectives range from bio-activity to toxicity. We report ROC_AUC for each dataset. The prediction pipeline is illustrated in Fig. 2e. Inspired by DeepEIK [15], we first obtain knowledge and text data for molecules within the dataset through SMILES matching. Then, we feed the multimodal inputs into MolFM. We concatenate the structure feature h^{SM} with the $[CLS]$ feature of the multimodal encoder. Finally, the multimodal feature is passed into a prediction head to fit the molecular property.

5 Experiments

In this section, we first conduct ablation studies to analyze the contributions of different components in MolFM (Sec. 5.1). Then, we present the state-of-the-art performance of MolFM on cross-modal retrieval (Sec. 5.2), molecule captioning (Sec. 5.3), text-to-molecule generation (Sec. 5.4) and molecular property prediction (Sec. 5.5). Furthermore, we showcase the implicit ability of our model to provide groundings through visualization of cross-modal attention (Sec. 5.6).

5.1 Ablation studies

To demonstrate the effectiveness of each component in MolFM, we compare performance on zero-shot cross-modal retrieval with different variants of our method in Tab. 1. We find that the application of re-ranking improves the retrieval performance. Surprisingly, the performance drops sharply when cross-modal attention to atoms or CMM is removed. These results highlight the significance of learning intricate connections between substructures and word snippets with a multi-modal encoder through appropriate pre-training tasks. Besides, incorporating knowledge graphs yields an average improvement of 1.5% for the same pre-training tasks, which demonstrates the effectiveness of global molecular knowledge. Furthermore, both attention to neighbors and KGE contributes slightly to MolFM’s capability to leverage knowledge graphs.

Table 1: Influence of MolFM components for zero-shot cross-modal retrieval. We report the average of R@1, R@5 and R@10. w/o knowledge: the knowledge graph input is removed. CMM: cross-modal matching. KGE: knowledge graph embedding.

Method	S-T	T-S
MolFM	26.27	28.78
- w/o re-rank	25.22	28.13
- w/o attention to atoms	23.45	25.89
- w/o attention to neighbors	25.23	28.49
- w/o knowledge	24.66	27.33
- w/o KGE	25.81	28.24
- w/o CMM	23.48	25.96
- w/o knowledge+CMM	22.07	24.48

Table 2: Paragraph-level cross-modal retrieval results on the test split of PCdes.

Mode	Model	S-T				T-S			
		MRR	R@1	R@5	R@10	MRR	R@1	R@5	R@10
zero-shot	MoMu [10]	9.89	5.08	12.82	18.93	10.33	4.90	14.48	20.69
	MolFM	21.42	13.90	28.69	36.21	23.63	16.14	30.67	39.54
fine-tune	SciBERT [27]	24.98	16.32	33.91	42.64	23.92	14.97	34.05	41.74
	KV-PLM [8]	27.41	18.35	37.15	45.43	25.97	16.55	35.85	44.75
	KV-PLM* [8]	29.15	20.60	37.87	45.74	28.12	19.29	37.33	45.29
	GraphMVP [23]	31.57	23.26	40.21	47.39	30.93	21.94	40.28	47.90
	MoMu [10]	34.29	24.47	45.38	53.84	34.53	24.87	44.93	54.25
	MolFM	39.56	29.76	50.53	58.63	39.34	29.39	50.26	58.49

Table 3: Molecule captioning results on the test split of ChEBI-20

Decoder	Encoder	BLEU-2	BLEU-4	ROUGE-1	ROUGE-2	ROUGE-L	METEOR	Text2Mol
MolT5-small	MolT5-small [9]	0.519	0.436	0.620	0.469	0.563	0.551	0.540
	MoMu [10]	0.532	0.445	0.621	0.469	0.564	0.557	0.543
	GraphMVP [23]	0.540	0.449	0.619	0.465	0.560	0.562	0.553
	MolFM	0.542	0.452	0.623	0.469	0.562	0.564	0.557
MolT5-base	MolT5-base [9]	0.540	0.457	0.634	0.485	0.578	0.569	0.547
	MoMu [10]	0.549	0.462	0.630	0.479	0.575	0.576	0.558
	GraphMVP [23]	0.577	0.491	0.651	0.505	0.592	0.599	0.570
	MolFM	0.585	0.498	0.653	0.508	0.594	0.607	0.576

5.2 Evaluation on cross-modal retrieval

Tab. 2 shows the overall cross-modal retrieval performance. Detailed results and analysis could be found in Appendix E and Appendix F.1. In the zero-shot setting, MolFM achieves a notable increase of 11.08% and 13.19% in MRR over the state-of-the-art method MoMu on S-T and T-S retrieval. In the fine-tuning setting, MolFM continues to deliver significant improvements. Given the limited scale and substantial noise of our pre-training dataset, we conclude that MolFM exhibits strong generalization capabilities in cross-modal retrieval tasks.

5.3 Evaluation on molecule captioning

Tab. 3 reports the results of molecule captioning, where MolFM consistently achieves state-of-the-art performance. Compared to MolT5 and MoMu, MolFM shows significant advancements in BLEU [51] and Text2Mol [16] measures, indicating that it generates smoother and more semantically related descriptions. In comparison to GraphMVP, MolFM also exhibits modest improvements, demonstrating that our multimodal pre-training further brings benefits to our structure encoder. Additionally, we provide molecule captioning examples in Fig. 3 and Appendix F.2. It is evident that MolFM shows better understanding of complex functional groups such as oligosaccharides and molecular properties such as inhibitory effects.

5.4 Evaluation on text-to-molecule generation

Tab. 4 shows the results on text-to-molecule generation. MolFM outperforms prior models by generating molecules with considerably higher exact ratio and fingerprint Tanimoto similarity. Qualitative results in Fig. 4 also demonstrate that MolFM is able to capture subtle differences between similar sub-structures. Further cases and analysis can be found in Appendix F.3.

5.5 Evaluation on molecular property prediction

Tab. 5 reports the performance comparison on molecular property prediction. By incorporating additional knowledge graphs and texts, MolFM achieves state-of-the-art performance across 6 out of 8 datasets, demonstrating an average absolute gain of 1.55% over GraphMVP. When considering inputs from a single modality, namely molecular structure, MolFM shows improved results on Tox21, ToxCast, MUV, HIV and BACE, no statistically significant difference on BBBP and ClinTox,

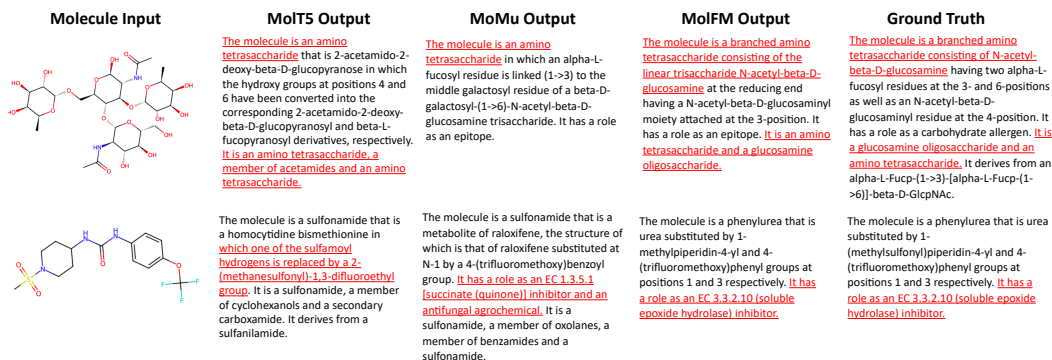


Figure 3: Molecule captioning examples. We highlight the text segments where MolFM generates more accurate expressions.

Table 4: Text-based molecule generation results on the test split of ChEBI-20. \uparrow : The higher the better. \downarrow : The lower the better.

Decoder	Encoder	BLEU \uparrow	Exact \uparrow	Valid \uparrow	Levenshtein \downarrow	MACCS FTS \uparrow	RDKit FTS \uparrow	Morgan FTS \uparrow	Text2Mol \uparrow
MolT5-small	MolT5-small [9]	0.749	0.081	0.724	29.160	0.780	0.653	0.601	0.533
	SciBERT [27]	0.797	0.142	0.846	22.027	0.818	0.695	0.639	0.561
	MoMu [10]	0.800	0.150	0.858	21.446	0.818	0.709	0.651	0.566
	MolFM	0.803	0.169	0.859	20.868	0.834	0.721	0.662	0.573
MolT5-base	MolT5-base [9]	0.779	0.082	0.786	25.188	0.787	0.661	0.601	0.543
	SciBERT [27]	0.812	0.179	0.852	21.192	0.844	0.733	0.678	0.575
	MoMu [10]	0.815	0.183	0.863	20.520	0.847	0.737	0.678	0.580
	MolFM	0.822	0.210	0.892	19.445	0.854	0.758	0.697	0.583

and a slight performance decrease on SIDER compared to GraphMVP. These results highlight the effectiveness of our pre-training, especially when leveraging multimodal information.

5.6 Visualization of cross-modal attention

We provide visualizations of our cross-modal attention between atoms, neighbors and texts in Fig. 5, Fig. 6 and Appendix G. We randomly select molecules and input phrases describing their substructures or properties, and display the attention maps of $[CLS]$ in the last cross attention layer of the multimodal encoder with a min-max normalization. Notably, the highlighted atoms in Fig. 5 form substructures that are strongly correlated to the text semantics. The multimodal attention in Fig. 6 also captures relevant entities based on textual descriptions. These results reveal the potential of MolFM to establish meaningful associations between structures, texts and knowledge graphs.

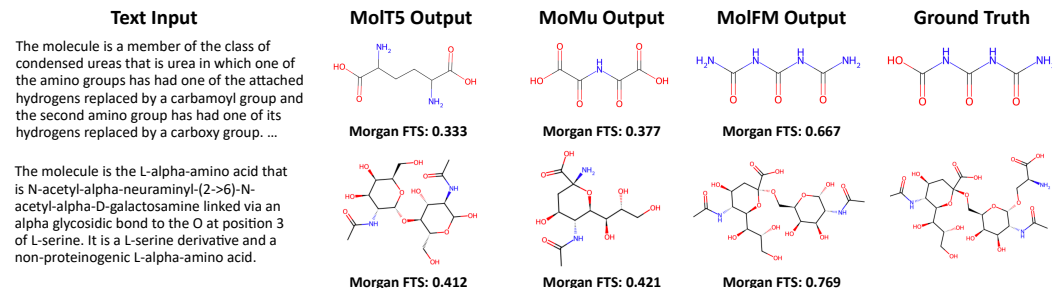


Figure 4: Examples of text-to-molecule generation examples, along with the Morgan fingerprint Tanimoto similarity between the generated molecules and the ground truth.

Table 5: Molecular property prediction results on MoleculeNet. w/o T+K: without the additional inputs from texts and knowledge graphs. w/ T+K: with the additional inputs from texts and knowledge graphs.

Model	BBBP	Tox21	ToxCast	SIDER	ClinTox	MUV	HIV	BACE	Avg
GIN	65.4 \pm 2.4	74.9 \pm 0.8	61.6 \pm 1.2	58.0 \pm 2.4	58.8 \pm 5.5	71.0 \pm 2.5	75.3 \pm 0.5	72.6 \pm 4.9	67.21
AttrMask [20]	70.2 \pm 0.5	74.2 \pm 0.8	62.5 \pm 0.4	60.4 \pm 0.6	68.6 \pm 9.6	73.9 \pm 1.3	74.3 \pm 0.6	77.2 \pm 1.4	70.16
ContextPred [20]	71.2 \pm 0.9	73.3 \pm 0.5	62.8 \pm 0.3	59.3 \pm 1.4	73.7 \pm 4.0	72.5 \pm 2.2	75.8 \pm 1.1	78.6 \pm 1.4	70.89
GraphCL [21]	67.5 \pm 3.3	75.0 \pm 0.3	62.8 \pm 0.2	60.1 \pm 1.3	78.9 \pm 4.2	77.1 \pm 1.0	75.0 \pm 0.4	68.7 \pm 7.8	70.64
GraphMVP [23]	72.4 \pm 1.6	74.4 \pm 0.2	63.1 \pm 0.4	63.9 \pm 1.2	77.5 \pm 4.2	75.0 \pm 1.0	77.0 \pm 1.2	81.2 \pm 0.9	73.07
KV-PLM [8]	66.9 \pm 1.1	64.7 \pm 1.8	58.6 \pm 0.4	55.3 \pm 0.8	84.3 \pm 1.5	60.2 \pm 2.9	68.8 \pm 4.9	71.9 \pm 2.1	66.29
DeepEIK [15]	72.1 \pm 0.4	72.4 \pm 0.9	61.5 \pm 0.4	63.5 \pm 0.9	89.7 \pm 1.8	71.4 \pm 1.0	75.0 \pm 0.6	80.5 \pm 1.2	73.27
MoMu [10]	70.5 \pm 2.0	75.6 \pm 0.3	63.4 \pm 0.5	60.5 \pm 0.9	79.9 \pm 4.1	70.5 \pm 1.4	75.9 \pm 0.8	76.7 \pm 2.1	71.63
MolFM (w/o T+K)	72.2 \pm 0.1	76.6 \pm 0.4	64.2 \pm 0.1	63.2 \pm 0.3	78.6 \pm 1.3	76.0 \pm 0.8	78.2 \pm 0.4	82.6 \pm 0.6	73.95
MolFM (w/ T+K)	72.9 \pm 0.1	77.2 \pm 0.7	64.4 \pm 0.2	64.2 \pm 0.9	79.7 \pm 1.6	76.0 \pm 0.8	78.8 \pm 1.1	83.9 \pm 1.1	74.62

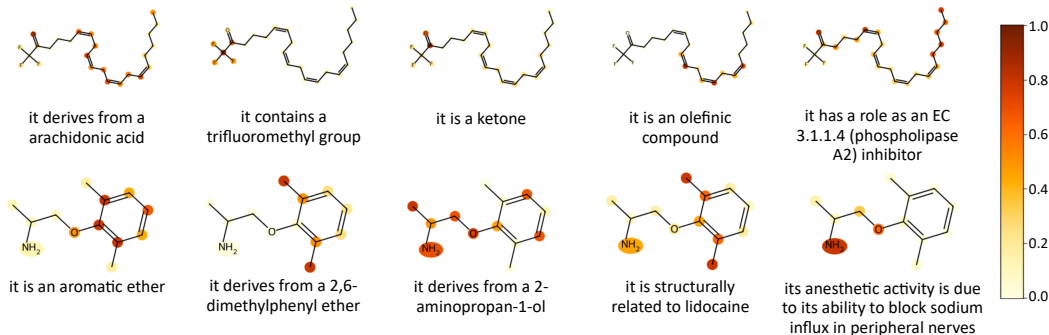


Figure 5: Visualization of atom attention with different input texts.

6 Limitations and broader impacts

While our work presents promising results in multi-modal molecular modeling, there are still areas for improvement and future exploration: (1) Our pre-training dataset may introduce biases or harmful information to MolFM due to its scale and quality. (2) MolFM may bring limited benefits to newly emerged molecules that lack available text and knowledge information. (3) While MolFM primarily focuses on molecules, incorporating other entities such as proteins, genes, and cell lines may lead to an even more comprehensive understanding of the biomedical context.

MolFM presents significant benefits for accelerating pharmaceutical research by connecting molecular structure with natural language and expert knowledge. However, there is a concern that MolFM may be misused to generate potentially dangerous or toxic molecules. Therefore, it is essential to ensure the responsible and ethical use of the model. We emphasize that MolFM should be employed solely for research purposes, and any further medical applications of MolFM should proceed with caution and undergo comprehensive experimental evaluations.

7 Conclusion

In this paper, we present MolFM, a multimodal molecular foundation model to facilitate joint representation learning with molecular structures, biomedical texts and knowledge graphs through

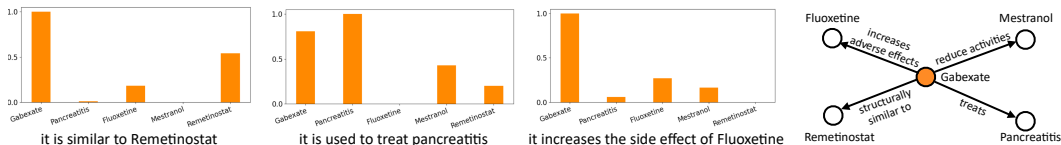


Figure 6: Visualization of neighbor attention. **Left:** the input text and the normalized attention value to different entities. **Right:** the selected molecule (orange) and the relationships with its one-hop neighbors.

leveraging fine-grained cross attention between three modalities. We demonstrate the effectiveness of our pre-training paradigm by both theoretical analysis and experimental evaluation. MolFM achieves state-of-the-art performance on various downstream tasks, with exceptional improvements in cross-modal retrieval. Under thorough analysis aimed at safety, MolFM has the potential to deliver unprecedented benefits to the biomedical research community.

Acknowledgments and Disclosure of Funding

This work is supported by the National Key R&D Program of China (No. 2022YFF1203002).

References

- [1] Jiasen Lu, Dhruv Batra, Devi Parikh, and Stefan Lee. Vilbert: Pretraining task-agnostic visiolinguistic representations for vision-and-language tasks. *Advances in neural information processing systems*, 32, 2019.
- [2] Chao Jia, Yinfei Yang, Ye Xia, Yi-Ting Chen, Zarana Parekh, Hieu Pham, Quoc Le, Yun-Hsuan Sung, Zhen Li, and Tom Duerig. Scaling up visual and vision-language representation learning with noisy text supervision. In *International Conference on Machine Learning*, pages 4904–4916. PMLR, 2021.
- [3] Alec Radford, Jong Wook Kim, Chris Hallacy, Aditya Ramesh, Gabriel Goh, Sandhini Agarwal, Girish Sastry, Amanda Askell, Pamela Mishkin, Jack Clark, et al. Learning transferable visual models from natural language supervision. In *International conference on machine learning*, pages 8748–8763. PMLR, 2021.
- [4] Yangguang Li, Feng Liang, Lichen Zhao, Yufeng Cui, Wanli Ouyang, Jing Shao, Fengwei Yu, and Junjie Yan. Supervision exists everywhere: A data efficient contrastive language-image pre-training paradigm. In *International Conference on Learning Representations*, 2022.
- [5] Junnan Li, Ramprasaath Selvaraju, Akhilesh Gotmare, Shafiq Joty, Caiming Xiong, and Steven Chu Hong Hoi. Align before fuse: Vision and language representation learning with momentum distillation. *Advances in neural information processing systems*, 34:9694–9705, 2021.
- [6] Zi-Yi Dou, Yichong Xu, Zhe Gan, Jianfeng Wang, Shuohang Wang, Lijuan Wang, Chenguang Zhu, Pengchuan Zhang, Lu Yuan, Nanyun Peng, et al. An empirical study of training end-to-end vision-and-language transformers. In *Proceedings of the IEEE/CVF Conference on Computer Vision and Pattern Recognition*, pages 18166–18176, 2022.
- [7] Weijie Su, Xizhou Zhu, Yue Cao, Bin Li, Lewei Lu, Furu Wei, and Jifeng Dai. Vi-bert: Pre-training of generic visual-linguistic representations. In *International Conference on Learning Representations*, 2020.
- [8] Zheni Zeng, Yuan Yao, Zhiyuan Liu, and Maosong Sun. A deep-learning system bridging molecule structure and biomedical text with comprehension comparable to human professionals. *Nature communications*, 13(1):862, 2022.
- [9] Carl Edwards, Tuan Lai, Kevin Ros, Garrett Honke, and Heng Ji. Translation between molecules and natural language. *arXiv preprint arXiv:2204.11817*, 2022.
- [10] Bing Su, Dazhao Du, Zhao Yang, Yujie Zhou, Jiangmeng Li, Anyi Rao, Hao Sun, Zhiwu Lu, and Ji-Rong Wen. A molecular multimodal foundation model associating molecule graphs with natural language. *arXiv preprint arXiv:2209.05481*, 2022.
- [11] Shengchao Liu, Weili Nie, Chengpeng Wang, Jiarui Lu, Zhuoran Qiao, Ling Liu, Jian Tang, Chaowei Xiao, and Anima Anandkumar. Multi-modal molecule structure-text model for text-based retrieval and editing. *arXiv preprint arXiv:2212.10789*, 2022.
- [12] Thin Nguyen, Hang Le, Thomas P Quinn, Tri Nguyen, Thuc Duy Le, and Svetha Venkatesh. Graphdta: predicting drug–target binding affinity with graph neural networks. *Bioinformatics*, 37(8):1140–1147, 2021.

- [13] Tiffany J Callahan, Ignacio J Tripodi, Harrison Pielke-Lombardo, and Lawrence E Hunter. Knowledge-based biomedical data science. *Annual review of biomedical data science*, 3:23–41, 2020.
- [14] David N Nicholson and Casey S Greene. Constructing knowledge graphs and their biomedical applications. *Computational and structural biotechnology journal*, 18:1414–1428, 2020.
- [15] Yizhen Luo, Kui Huang, Massimo Hong, Kai Yang, Jiahuan Zhang, Yushuai Wu, and Zaiqin Nie. Empowering ai drug discovery with explicit and implicit knowledge. *arXiv preprint arXiv:2305.01523*, 2023.
- [16] Carl Edwards, ChengXiang Zhai, and Heng Ji. Text2mol: Cross-modal molecule retrieval with natural language queries. In *Proceedings of the 2021 Conference on Empirical Methods in Natural Language Processing*, pages 595–607, 2021.
- [17] Zhenqin Wu, Bharath Ramsundar, Evan N Feinberg, Joseph Gomes, Caleb Geniesse, Aneesh S Pappu, Karl Leswing, and Vijay Pande. Moleculenet: a benchmark for molecular machine learning. *Chemical science*, 9(2):513–530, 2018.
- [18] Seyone Chithrananda, Gabriel Grand, and Bharath Ramsundar. Chemberta: Large-scale self-supervised pretraining for molecular property prediction. *arXiv preprint arXiv:2010.09885*, 2020.
- [19] Ross Irwin, Spyridon Dimitriadis, Jiazhen He, and Esben Jannik Bjerrum. Chemformer: a pre-trained transformer for computational chemistry. *Machine Learning: Science and Technology*, 3(1):015022, 2022.
- [20] Weihua Hu, Bowen Liu, Joseph Gomes, Marinka Zitnik, Percy Liang, Vijay Pande, and Jure Leskovec. Strategies for pre-training graph neural networks. In *International Conference on Learning Representations*, 2020.
- [21] Yuning You, Tianlong Chen, Yongduo Sui, Ting Chen, Zhangyang Wang, and Yang Shen. Graph contrastive learning with augmentations. *Advances in neural information processing systems*, 33: 5812–5823, 2020.
- [22] Yuyang Wang, Jianren Wang, Zhonglin Cao, and Amir Barati Farimani. Molecular contrastive learning of representations via graph neural networks. *Nature Machine Intelligence*, 4(3):279–287, 2022.
- [23] Shengchao Liu, Hanchen Wang, Weiyang Liu, Joan Lasenby, Hongyu Guo, and Jian Tang. Pre-training molecular graph representation with 3d geometry. In *ICLR 2022 Workshop on Geometrical and Topological Representation Learning*, 2022.
- [24] Shengchao Liu, Hanchen Wang, Weiyang Liu, Joan Lasenby, Hongyu Guo, and Jian Tang. Pre-training molecular graph representation with 3d geometry. *arXiv preprint arXiv:2110.07728*, 2021.
- [25] Jinhua Zhu, Yingce Xia, Lijun Wu, Shufang Xie, Tao Qin, Wengang Zhou, Houqiang Li, and Tie-Yan Liu. Unified 2d and 3d pre-training of molecular representations. In *Proceedings of the 28th ACM SIGKDD Conference on Knowledge Discovery and Data Mining*, pages 2626–2636, 2022.
- [26] Hannes Stärk, Dominique Beaini, Gabriele Corso, Prudencio Tossou, Christian Dallago, Stephan Günnemann, and Pietro Liò. 3d infomax improves gnns for molecular property prediction. In *International Conference on Machine Learning*, pages 20479–20502. PMLR, 2022.
- [27] Iz Beltagy, Kyle Lo, and Arman Cohan. Scibert: A pretrained language model for scientific text. In *Proceedings of the 2019 Conference on Empirical Methods in Natural Language Processing and the 9th International Joint Conference on Natural Language Processing (EMNLP-IJCNLP)*, pages 3615–3620, 2019.
- [28] Jinhyuk Lee, Wonjin Yoon, Sungdong Kim, Donghyeon Kim, Sunkyu Kim, Chan Ho So, and Jaewoo Kang. Biobert: a pre-trained biomedical language representation model for biomedical text mining. *Bioinformatics*, 36(4):1234–1240, 2020.

- [29] Yu Gu, Robert Tinn, Hao Cheng, Michael Lucas, Naoto Usuyama, Xiaodong Liu, Tristan Naumann, Jianfeng Gao, and Hoifung Poon. Domain-specific language model pretraining for biomedical natural language processing. *ACM Transactions on Computing for Healthcare (HEALTH)*, 3(1):1–23, 2021.
- [30] Chih-Hsuan Wei, Yifan Peng, Robert Leaman, Allan Peter Davis, Carolyn J Mattingly, Jiao Li, Thomas C Wiegers, and Zhiyong Lu. Assessing the state of the art in biomedical relation extraction: overview of the biocreative v chemical-disease relation (cdr) task. *Database*, 2016, 2016.
- [31] Jacob Devlin, Ming-Wei Chang, Kenton Lee, and Kristina Toutanova. Bert: Pre-training of deep bidirectional transformers for language understanding. In *Proceedings of the 2019 Conference of the North American Chapter of the Association for Computational Linguistics: Human Language Technologies, Volume 1 (Long and Short Papers)*, pages 4171–4186, 2019.
- [32] Colin Raffel, Noam Shazeer, Adam Roberts, Katherine Lee, Sharan Narang, Michael Matena, Yanqi Zhou, Wei Li, and Peter J Liu. Exploring the limits of transfer learning with a unified text-to-text transformer. *The Journal of Machine Learning Research*, 21(1):5485–5551, 2020.
- [33] Wen Zhang, Yanlin Chen, Feng Liu, Fei Luo, Gang Tian, and Xiaohong Li. Predicting potential drug-drug interactions by integrating chemical, biological, phenotypic and network data. *BMC bioinformatics*, 18(1):1–12, 2017.
- [34] Maha A Thafar, Rawan S Olayan, Haitham Ashoor, Somayah Albaradei, Vladimir B Bajic, Xin Gao, Takashi Gojobori, and Magbubah Essack. DTiGEMS+: drug–target interaction prediction using graph embedding, graph mining, and similarity-based techniques. *Journal of Cheminformatics*, 12(1):1–17, 2020.
- [35] Qing Ye, Chang-Yu Hsieh, Ziyi Yang, Yu Kang, Jiming Chen, Dongsheng Cao, Shibo He, and Tingjun Hou. A unified drug–target interaction prediction framework based on knowledge graph and recommendation system. *Nature communications*, 12(1):1–12, 2021.
- [36] Mengying Sun, Jing Xing, Huijun Wang, Bin Chen, and Jiayu Zhou. Mocl: Data-driven molecular fingerprint via knowledge-aware contrastive learning from molecular graph. In *Proceedings of the 27th ACM SIGKDD Conference on Knowledge Discovery & Data Mining*, pages 3585–3594, 2021.
- [37] Yin Fang, Qiang Zhang, Haihong Yang, Xiang Zhuang, Shumin Deng, Wen Zhang, Ming Qin, Zhuo Chen, Xiaohui Fan, and Huajun Chen. Molecular contrastive learning with chemical element knowledge graph. In *Proceedings of the AAAI Conference on Artificial Intelligence*, volume 36, pages 3968–3976, 2022.
- [38] Keyulu Xu, Weihua Hu, Jure Leskovec, and Stefanie Jegelka. How powerful are graph neural networks? In *International Conference on Learning Representations*, 2018.
- [39] Ashish Vaswani, Noam Shazeer, Niki Parmar, Jakob Uszkoreit, Llion Jones, Aidan N Gomez, Łukasz Kaiser, and Illia Polosukhin. Attention is all you need. *Advances in neural information processing systems*, 30, 2017.
- [40] Antoine Bordes, Nicolas Usunier, Alberto Garcia-Duran, Jason Weston, and Oksana Yakhnenko. Translating embeddings for modeling multi-relational data. *Advances in neural information processing systems*, 26, 2013.
- [41] James Kirkpatrick, Razvan Pascanu, Neil Rabinowitz, Joel Veness, Guillaume Desjardins, Andrei A Rusu, Kieran Milan, John Quan, Tiago Ramalho, Agnieszka Grabska-Barwinska, et al. Overcoming catastrophic forgetting in neural networks. *Proceedings of the national academy of sciences*, 114(13):3521–3526, 2017.
- [42] Aaron van den Oord, Yazhe Li, and Oriol Vinyals. Representation learning with contrastive predictive coding. *arXiv preprint arXiv:1807.03748*, 2018.
- [43] Elad Hoffer and Nir Ailon. Deep metric learning using triplet network. In *Similarity-Based Pattern Recognition: Third International Workshop, SIMBAD 2015, Copenhagen, Denmark, October 12-14, 2015. Proceedings 3*, pages 84–92. Springer, 2015.

- [44] Mahmut Kaya and Hasan Şakir Bilge. Deep metric learning: A survey. *Symmetry*, 11(9):1066, 2019.
- [45] Sunghwan Kim, Paul A Thiessen, Evan E Bolton, Jie Chen, Gang Fu, Asta Gindulyte, Lianyi Han, Jane He, Siqian He, Benjamin A Shoemaker, et al. Pubchem substance and compound databases. *Nucleic acids research*, 44(D1):D1202–D1213, 2016.
- [46] Kyle Lo, Lucy Lu Wang, Mark Neumann, Rodney Kinney, and Daniel S Weld. S2orc: The semantic scholar open research corpus. In *Proceedings of the 58th Annual Meeting of the Association for Computational Linguistics*, pages 4969–4983, 2020.
- [47] David S Wishart, Yannick D Feunang, An C Guo, Elvis J Lo, Ana Marcu, Jason R Grant, Tanvir Sajed, Daniel Johnson, Carin Li, Zinat Sayeeda, et al. Drugbank 5.0: a major update to the drugbank database for 2018. *Nucleic acids research*, 46(D1):D1074–D1082, 2018.
- [48] Michael K Gilson, Tiqing Liu, Michael Baitaluk, George Nicola, Linda Hwang, and Jenny Chong. Bindingdb in 2015: a public database for medicinal chemistry, computational chemistry and systems pharmacology. *Nucleic acids research*, 44(D1):D1045–D1053, 2016.
- [49] Maxime Delmas, Olivier Filangi, Nils Paulhe, Florence Vinson, Christophe Duperier, William Garrier, Paul-Emeric Saunier, Yoann Pitarch, Fabien Jourdan, Franck Giacomoni, et al. building a knowledge graph from public databases and scientific literature to extract associations between chemicals and diseases. *Bioinformatics*, 37(21):3896–3904, 2021.
- [50] Ilya Loshchilov and Frank Hutter. Decoupled weight decay regularization. *arXiv preprint arXiv:1711.05101*, 2017.
- [51] Kishore Papineni, Salim Roukos, Todd Ward, and Wei-Jing Zhu. Bleu: a method for automatic evaluation of machine translation. In *Proceedings of the 40th annual meeting of the Association for Computational Linguistics*, pages 311–318, 2002.

Appendix

A Theoretical justifications for MolFM pre-training

In this section, we establish a connection between our pre-training objectives and deep metric learning. We first show that MolFM aligns the feature space for different modalities of the same molecule by analyzing structure-text contrastive (Sec. A.1), masked language model (Sec. A.2) and cross-modal matching (Sec. A.3). Then, we give detailed proofs for two lemmas presented in the main document, demonstrating that MolFM grasps global molecular expertise including structural and functional similarity (Sec. A.4).

A.1 Analysis of structure-text contrastive (STC) loss

Given a set of triplets (x, y, z) where x is the anchor sample, y is the positive sample that shares semantic correlations with x , and z is the negative sample, deep metric learning [1, 2] aims to learn a representation network $\mathcal{F}_\Theta(\cdot)$ and a distance metric function $\mathcal{D}_\beta(\cdot, \cdot)$ that minimizes the distance between $\mathcal{F}_\Theta(x)$ and $\mathcal{F}_\Theta(y)$ and maximizes the distance between $\mathcal{F}_\Theta(x)$ and $\mathcal{F}_\Theta(z)$:

$$\arg \min_{\Theta, \beta} \mathbb{E}_{(x, y, z)} [\mathcal{D}_\beta(\mathcal{F}_\Theta(x), \mathcal{F}_\Theta(y)) - \mathcal{D}_\beta(\mathcal{F}_\Theta(x), \mathcal{F}_\Theta(z))], \quad (\text{A.1})$$

where Θ and β are model parameters.

It has been well studied that optimizing the InfoNCE loss is equivalent to maximizing a lower bound of the mutual information between two different views of a data point [3, 4]:

$$I(A; B) \geq -\mathcal{L}_{NCE} = \mathbb{E}_{(a, b)} \left[\log \frac{\exp(s(a, b))}{\sum_{\tilde{b} \in \tilde{B}} \exp(s(a, \tilde{b}))} \right], \quad (\text{A.2})$$

where A, B are random variables for the embeddings of different views, a, b are positive samples, $I(\cdot; \cdot)$ denotes mutual information, $s(\cdot, \cdot)$ is a scoring function (we use cosine similarity in this study), and \tilde{B} is a proposal distribution that contains b and $|\tilde{B}| - 1$ data points. Following [5], we connect InfoNCE loss in Eq. A.2 with deep metric learning by approximating $\log(1 + x)$ as x and first-order Taylor expansion:

$$\begin{aligned} -\mathbb{E}_{(a, b)} \left[\log \frac{\exp(s(a, b))}{\sum_{\tilde{b} \in \tilde{B}} \exp(s(a, \tilde{b}))} \right] &= \mathbb{E}_{(a, b)} \left[\log \left(1 + \sum_{\tilde{b} \in \tilde{B}, \tilde{b} \neq b} \exp(s(a, \tilde{b}) - s(a, b)) \right) \right] \\ &\approx \mathbb{E}_{(a, b)} \left[\sum_{\tilde{b} \in \tilde{B}, \tilde{b} \neq b} \exp(s(a, \tilde{b}) - s(a, b)) \right] \\ &\propto -\mathbb{E}_{(a, b)} \left[\sum_{\tilde{b} \in \tilde{B}} [s(a, b) - s(a, \tilde{b})] \right]. \end{aligned} \quad (\text{A.3})$$

By conceptualizing $-s(\cdot, \cdot)$ as the metric function, the equation above establishes the connection between contrastive learning and deep metric learning.

Hence, assuming the projection head is an identical mapping, our structure-text contrastive (STC) aligns structural and textual representations for the same molecule in the following:

$$\begin{aligned} \mathcal{L}_{stc} &= -\frac{1}{2} \mathbb{E}_{(S, T, K)} \left[\log \frac{\exp(s(z_S, z_T)/\tau)}{\sum_{S' \in B} \exp(s(z_{S'}, z_T)/\tau)} + \log \frac{\exp(s(z_S, z_{T'})/\tau)}{\sum_{T' \in B} \exp(s(z_S, z_{T'})/\tau)} \right] \\ &\propto -\frac{1}{2\tau} \mathbb{E}_{(S, T, K)} \left[\sum_{S' \in B} [s(h_S, h_T) - s(h_{S'}, h_T)] + \sum_{T' \in B} [s(h_S, h_T) - s(h_S, h_{T'})] \right], \end{aligned} \quad (\text{A.4})$$

where B consists of molecular structures and texts within the same mini-batch, and τ is a temperature hyper-parameter.

A.2 Analysis of masked language model (MLM)

Following [4], we rewrite masked language modeling loss based on Eq. A.3 in the following:

$$\begin{aligned}
\mathcal{L}_{mlm} &= \mathbb{E}_{(S, \hat{T}, K)} \left[H(y_{mlm}(\hat{T}), p_{mlm}(\mathcal{M}_\theta(h_S, h_{\hat{T}}, h_K))) \right] \\
&= -\mathbb{E}_{(S, \hat{T}, K)} \left[\log \frac{\exp[s(y_{mlm}(\hat{T}), p_{mlm}(\mathcal{M}_\theta(h_S, h_{\hat{T}}, h_K)))]}{\sum_{y \in \mathcal{V}} \exp[s(\psi(y), p_{mlm}(\mathcal{M}_\theta(h_S, h_{\hat{T}}, h_K)))]} \right] \\
&\propto -\mathbb{E}_{(S, \hat{T}, K)} \left[\sum_{y \in \mathcal{V}} [s(y_{mlm}(\hat{T}), p_{mlm}(\mathcal{M}_\theta(h_S, h_{\hat{T}}, h_K))) \right. \\
&\quad \left. - s(\psi(y), p_{mlm}(\mathcal{M}_\theta(h_S, h_{\hat{T}}, h_K))) \right], \tag{A.5}
\end{aligned}$$

where \hat{T} is the masked token sequence, $y_{mlm}(\hat{T})$ is the one-hot ground truth of the masked token, \mathcal{M}_θ is the multi-modal encoder, p_{mlm} is a predictor that calculates the probability distribution for masked tokens, and $\psi(\cdot) : \mathcal{V} \rightarrow \mathbb{R}^{|\mathcal{V}|}$ is a function that maps tokens in the vocabulary set \mathcal{V} to one-hot encodings. Hence, MLM pulls close representations between masked tokens with their multi-modal context.

A.3 Analysis of cross-modal matching (CMM)

Based on Eq. A.3, the cross-modal matching loss is equivalent to the following:

$$\begin{aligned}
\mathcal{L}_{cmm} &= \mathbb{E}_{(S, T, K)} \left[\sum_{(\tilde{S}, \tilde{T}, \tilde{K}) \in \tilde{B}} H(y_{cmm}(\tilde{S}, \tilde{T}, \tilde{K}), p_{cmm}(\mathcal{M}_\theta(h_{\tilde{S}}, h_{\tilde{T}}, h_{\tilde{K}}))) \right] \\
&= -\mathbb{E}_{(S, T, K)} \left[\log \frac{\exp[p_{cmm}(\mathcal{M}_\theta(h_S, h_T, h_K))]}{\sum_{(\tilde{S}, \tilde{T}, \tilde{K}) \in \tilde{B}} \exp[p_{cmm}(\mathcal{M}_\theta(h_{\tilde{S}}, h_{\tilde{T}}, h_{\tilde{K}}))]} \right] \\
&\propto - \sum_{(\tilde{S}, \tilde{T}, \tilde{K}) \in \tilde{B}} [p_{cmm}(\mathcal{M}_\theta(h_S, h_T, h_K)) - p_{cmm}(\mathcal{M}_\theta(h_{\tilde{S}}, h_{\tilde{T}}, h_{\tilde{K}}))], \tag{A.6}
\end{aligned}$$

where \tilde{B} is the corrupted mini-batch with $y_{cmm}(\tilde{S}, \tilde{T}, \tilde{K})$ indicating whether the multimodal data from the mini-batch correspond to the same molecule, and p_{cmm} is a binary predictor. By conceptualizing $-p_{cmm}(\mathcal{M}_\theta(\cdot, \cdot, \cdot))$ as a distance function, we demonstrate that CMM aligns the structural, textual and knowledge graph representations of the same molecule.

A.4 Analysis of knowledge graph embedding (KGE)

In this sub-section, we start with several definitions and denotations with respect to the knowledge graph embedding algorithm. Then we prove the two lemmas in the main document, showing that KGE pulls close embeddings for molecules that shares similar structures (Lemma. A.1) or similar functions (Lemma. A.2).

Definition A.1. *Knowledge Graph Embedding.* We define $KG = \{(h, r, t) | h, t \in \mathcal{E}, r \in \mathcal{R}\}$ where \mathcal{E} is the entity set and \mathcal{R} is the relation set. We define $N = |\mathcal{E}|$ (the number of entities) and $M = |\mathcal{R}|$ (the number of relations), and use $x \sim X$ to denote that x is uniformly sampled from X . KGE aims to learn an entity embedding function $f : \mathcal{E} \rightarrow \mathbb{R}^n$ and a relation embedding function $g : \mathcal{R} \rightarrow \mathbb{R}^n$ by optimizing the following max-of-margin loss for each triplet $(h, r, t) \in KG$:

$$\begin{aligned}
\mathcal{L}_{kge}(h, r, t) &= \mathbb{E}_{\tilde{t} \sim \mathcal{E} \setminus t} [\max(0, d(h, r, t) - d(h, r, \tilde{t}) + \Delta)] \\
&\quad + \mathbb{E}_{\tilde{h} \sim \mathcal{E} \setminus h} [\max(0, d(h, r, t) - d(\tilde{h}, r, t) + \Delta)], \tag{A.7}
\end{aligned}$$

where $d(h, r, t) = \|f(h) + g(r) - f(t)\|_2$ is a distance function and Δ is a margin hyper-parameter.

Definition A.2. Given a subset $\mathcal{T} \subset KG$, assume that $\mathcal{X}_{h,r,t} = 1$ indicates $(h, r, t) \in \mathcal{T}$ and $\mathcal{X}_{h,r,t} = 0$ indicates $(h, r, t) \notin \mathcal{T}$. We define $d_{h,r}^{\text{out}} = \sum_{t \in \mathcal{E}} \mathcal{X}_{h,r,t}$ as the out-degree of h under relation r with respect to \mathcal{T} , and $d_{t,r}^{\text{in}} = \sum_{h \in \mathcal{E}} \mathcal{X}_{h,r,t}$ as the in-degree of t under relation r with respect to \mathcal{T} .

We further give the following assumptions:

Assumption 1. $\Delta > d(h_1, r_1, t_1) - d(h_2, r_2, t_2)$ for all $h_1, t_1, h_2, t_2 \in \mathcal{E}$ and $r_1, r_2 \in \mathcal{R}$.

Definition A.3. Structurally similar molecules. Assume that $h, t \in \mathcal{E}$ are two molecular entities, and $r_s \in \mathcal{R}$ is a relation type indicating structural similarity. h and t are structurally similar if and only if $(h, r_s, t) \in KG$ and $(t, r_s, h) \in KG$. We use $S = \{(h, r_s, t) | (h, r_s, t) \in KG\}$ to denote the set of structural similar relations and assume that $|S| \geq 4$.

Assumption 2. Symmetry of r_s : $\forall h, t \in \mathcal{E}, (h, r_s, t) \in KG \Leftrightarrow (t, r_s, h) \in KG$.

Assumption 3. Isotropy of r_s : $f(h) + g(r_s) - f(t)$ is uniformly distributed in all directions for $(h, r_s, t) \in S$ or arbitrary $h, t \in \mathcal{E}$. Further, we use $\alpha_{(h,r_s,t)}$ to denote the angle between an arbitrary vector x and $f(t) + g(r_s) - f(h)$, and hypothesize that for all $x \in \mathbb{R}^d$, the following holds:

$$\begin{aligned} -\epsilon &\leq \sum_{(h,r_s,t) \in S} \frac{\cos 2\alpha_{(h,r_s,t)}}{d(h, r_s, t)} \leq \epsilon, \\ -\epsilon &\leq \sum_{h,t \in \mathcal{E}} \frac{\cos 2\alpha_{(h,r_s,t)}}{d(h, r_s, t)} \leq \epsilon, \end{aligned} \quad (\text{A.8})$$

where $\epsilon > 0$ is a constant that is close to 0.

Assumption 4. Sparsity of r_s : $d_{h,r_s}^{\text{out}} \leq \frac{N}{2}$ and $d_{t,r_s}^{\text{in}} \leq \frac{N}{2}$ for all $h, t \in \mathcal{E}$.

Assumption 5. Distance margin between positive and negative samples. If $(h, r_s, t) \in KG$, $(h, r_s, \tilde{t}) \notin KG$ and $(\tilde{h}, r_s, t) \notin KG$, the following holds:

$$\frac{1}{d(h, r_s, t)} - \frac{1}{d(h, r_s, \tilde{t})} \geq \epsilon, \quad \frac{1}{d(h, r_s, t)} - \frac{1}{d(\tilde{h}, r_s, t)} \geq \epsilon.$$

Lemma A.1. For structurally similar molecules h and t , the following holds:

$$\mathcal{L}_{\text{KGE}}(h, r_s, t) \propto 2\|f(h) - f(t)\|_2 - \mathbb{E}_{\tilde{t} \sim \mathcal{E} \setminus t} \|f(h) - f(\tilde{t})\|_2 - \mathbb{E}_{\tilde{h} \sim \mathcal{E} \setminus h} \|f(\tilde{h}) - f(t)\|_2. \quad (\text{A.9})$$

Proof. Our proof sketch is showing that optimizing KGE substantially leads to $g(r_s) = 0$. Formally:

$$\arg \min_{g(r_s)} \mathbb{E}_{(h,r,t) \sim KG} [\mathcal{L}_{\text{KGE}}(h, r, t)] = 0. \quad (\text{A.10})$$

We first rewrite Eq. A.7 in the following based on Assumption 1:

$$\begin{aligned} \mathcal{L} &= \mathbb{E}_{(h,r,t) \sim KG} [\mathcal{L}_{\text{KGE}}(h, r, t)] \\ &= \frac{|S|}{M} \sum_{(h,r_s,t) \in S} \left[2d(h, r_s, t) - \mathbb{E}_{\tilde{t} \sim \mathcal{E} \setminus t} [d(h, r_s, \tilde{t})] - \mathbb{E}_{\tilde{h} \sim \mathcal{E} \setminus h} [d(\tilde{h}, r_s, t)] \right] \\ &\quad + \frac{M - |S|}{M} \sum_{(h,r,t) \in KG \setminus S} \left[2d(h, r, t) - \mathbb{E}_{\tilde{t} \sim \mathcal{E} \setminus t} [d(h, r, \tilde{t})] - \mathbb{E}_{\tilde{h} \sim \mathcal{E} \setminus h} [d(\tilde{h}, r, t)] \right]. \end{aligned} \quad (\text{A.11})$$

Following [6], we rewrite negative sampling terms as follows:

$$\begin{aligned} \sum_{(h,r,t) \in S} \mathbb{E}_{\tilde{t} \sim \mathcal{E} \setminus t} [d(h, r, \tilde{t})] &= \frac{1}{N-1} \sum_{(h,r,t) \in S} \left[-d(h, r, t) + \sum_{\tilde{t} \in \mathcal{E}} d(h, r, \tilde{t}) \right] \\ &= \sum_{h,t \in \mathcal{E}, r \in \mathcal{R}} \frac{d_{h,r}^{\text{out}}}{N-1} d(h, r, t) - \frac{1}{N-1} \sum_{(h,r,t) \in S} d(h, r, t), \end{aligned} \quad (\text{A.12})$$

and:

$$\sum_{(h,r,t) \in S} \mathbb{E}_{\tilde{h} \sim \mathcal{E} \setminus h} [d(\tilde{h}, r, t)] = \sum_{h,t \in \mathcal{E}, r \in \mathcal{R}} \frac{d_{t,r}^{\text{in}}}{N-1} d(h, r, t) - \frac{1}{N-1} \sum_{(h,r,t) \in KG} d(h, r, t), \quad (\text{A.13})$$

Due to the symmetry of r_s (Assumption 2), we can derive that $d_{h,r_s}^{out} = d_{h,r_s}^{in}$ for all $h \in \mathcal{E}$.

As suggested in [7], we speculate a value independence for each $r \in \mathcal{R}$ given sufficient large embedding dimension n . Hence, we calculate the partial derivative with $g(r_s)$ as follows:

$$\begin{aligned}
\frac{\partial \mathcal{L}}{\partial g(r_s)} &= \frac{2|S|N}{M(N-1)} \sum_{(h,r_s,t) \in S} \frac{\partial d(h, r_s, t)}{\partial g(r_s)} - \frac{|S|}{|M|(N-1)} \sum_{h,t \in \mathcal{E}} (d_{h,r_s}^{out} + d_{t,r_s}^{in}) \frac{\partial d(h, r_s, t)}{\partial g(r_s)} \\
&= \frac{2|S|N}{M(N-1)} \sum_{(h,r_s,t) \in S} \frac{f(h) + g(r_s) - h(t)}{d(h, r_s, t)} \\
&\quad - \frac{|S|}{|M|(N-1)} \sum_{h,t \in \mathcal{E}} (d_{h,r_s}^{out} + d_{t,r_s}^{in}) \frac{f(h) + g(r_s) - f(t)}{d(h, r_s, t)} \\
&= \gamma N \sum_{(h,r_s,t) \in S} \left[\frac{f(h) + g(r_s) - f(t)}{d(h, r_s, t)} + \frac{f(t) + g(r_s) - f(h)}{d(t, r_s, h)} \right] \\
&\quad - \frac{\gamma}{2} \sum_{h,t \in \mathcal{E}} \left[(d_{h,r_s}^{out} + d_{t,r_s}^{in}) \frac{f(h) + g(r_s) - f(t)}{d(h, r_s, t)} + (d_{t,r_s}^{out} + d_{h,r_s}^{in}) \frac{f(t) + g(r_s) - f(h)}{d(t, r_s, h)} \right] \\
&= \gamma N \sum_{(h,r_s,t) \in S} \left[\frac{f(h) + g(r_s) - f(t)}{d(h, r_s, t)} + \frac{f(t) + g(r_s) - f(h)}{d(t, r_s, h)} \right] \\
&\quad - \frac{\gamma}{2} \sum_{h,t \in \mathcal{E}} (d_{h,r_s}^{out} + d_{t,r_s}^{in}) \left[\frac{f(h) + g(r_s) - f(t)}{d(h, r_s, t)} + \frac{f(t) + g(r_s) - f(h)}{d(t, r_s, h)} \right], \tag{A.14}
\end{aligned}$$

where $\gamma = \frac{2|S|}{M(N-1)}$. If $g(r_s) = 0$, we can derive that $d(h, r_s, t) = \|h - t\|_2 = d(t, r_s, h)$ and that $\frac{\partial \mathcal{L}}{\partial g(r_s)} = 0$.

We further calculate the Hessian matrix \mathcal{H} in the following:

$$\begin{aligned}
\mathcal{H} &= \frac{\partial^2 \mathcal{L}}{\partial g(r_s)^2} \\
&= \gamma N \sum_{(h,r_s,t) \in S} \frac{\partial^2 d(h, r_s, t)}{\partial g(r_s)^2} - \frac{\gamma}{2} \sum_{h,t \in \mathcal{E}} (d_{h,r_s}^{out} + d_{t,r_s}^{in}) \frac{\partial^2 d(h, r_s, t)}{\partial g(r_s)^2} \\
&= \gamma N \sum_{(h,r_s,t) \in S} \frac{d^2(h, r_s, t)I - [f(t) + g(r_s) - f(h)][f(t) + g(r_s) - f(h)]^T}{d^3(h, r_s, t)} \\
&\quad - \frac{\gamma}{2} \sum_{h,t \in \mathcal{E}} (d_{h,r_s}^{out} + d_{t,r_s}^{in}) \frac{d^2(h, r_s, t)I - [f(t) + g(r_s) - f(h)][f(t) + g(r_s) - f(h)]^T}{d^3(h, r_s, t)}. \tag{A.15}
\end{aligned}$$

For an arbitrary vector $x \in \mathbb{R}^d$ of unit length ($\|x\|_2 = 1$), we show that:

$$\begin{aligned}
x^T \mathcal{H} x &= \gamma N \sum_{(h, r_s, t) \in S} \frac{d^2(h, r_s, t) x^T x - (x^T [f(t) + g(r_s) - f(h)])^2}{d^3(h, r_s, t)} \\
&\quad - \frac{\gamma}{2} \sum_{h, t \in \mathcal{E}} (d_{h, r_s}^{\text{out}} + d_{t, r_s}^{\text{in}}) \frac{d^2(h, r_s, t) x^T x - (x^T [f(t) + g(r_s) - f(h)])^2}{d^3(h, r_s, t)} \\
&= \gamma N \sum_{(h, r_s, t) \in S} \frac{1 - s^2(x, f(t) + g(r_s) - f(h))}{d(h, r_s, t)} \\
&\quad - \frac{\gamma}{2} \sum_{h, t \in \mathcal{E}} (d_{h, r_s}^{\text{out}} + d_{t, r_s}^{\text{in}}) \frac{1 - s^2(x, f(t) + g(r_s) - f(h))}{d(h, r_s, t)} \\
&= \frac{\gamma N}{2} \sum_{(h, r_s, t) \in S} \frac{1 - \cos 2\alpha(h, r_s, t)}{d(h, r_s, t)} - \frac{\gamma}{4} \sum_{h, t \in \mathcal{E}} (d_{h, r_s}^{\text{out}} + d_{t, r_s}^{\text{in}}) \frac{1 - \cos 2\alpha(h, r_s, t)}{d(h, r_s, t)} \\
&\geq \frac{\gamma N}{2} \sum_{(h, r_s, t) \in S} \frac{1}{d(h, r_s, t)} - \frac{\gamma}{4} \sum_{h, t \in \mathcal{E}} (d_{h, r_s}^{\text{out}} + d_{t, r_s}^{\text{in}}) \frac{1}{d(h, r_s, t)} - \frac{3}{4} \gamma N \epsilon \tag{A.16} \\
&= \frac{\gamma}{4} \left[\sum_{(h, r_s, t) \in S} \left[\sum_{\tilde{t} \in \mathcal{E}, (h, r_s, \tilde{t}) \notin S} \left(\frac{1}{d(h, r_s, t)} - \frac{1}{d(h, r_s, \tilde{t})} \right) \right. \right. \\
&\quad \left. \left. + \sum_{\tilde{h} \in \mathcal{E}, (\tilde{h}, r_s, t) \notin S} \left(\frac{1}{d(h, r_s, t)} - \frac{1}{d(\tilde{h}, r_s, t)} \right) \right] \right] - \frac{3}{4} \gamma N \epsilon \\
&\geq \frac{\gamma}{4} (2N - d_{h, r_s}^{\text{out}} - d_{t, r_s}^{\text{in}}) \epsilon - \frac{3}{4} \gamma N \epsilon \\
&\geq \frac{\gamma N |S| \epsilon}{4} - \frac{3}{4} \gamma N \epsilon \\
&\geq 0,
\end{aligned}$$

where $s(\cdot, \cdot)$ is cosine similarity. Eq. A.16 shows that $\frac{\partial^2 \mathcal{L}}{\partial g(r_s)^2}$ is positive definite for any $g(r_s) \in \mathbb{R}^d$. Therefore, $g(r_s) = 0$ is the minimum point of \mathcal{L} .

Finally we derive the following based on Assumption 1:

$$\begin{aligned}
\mathcal{L}_{\text{kgc}}(h, r_s, t) &= \mathbb{E}_{\tilde{t} \sim \mathcal{E} \setminus t} [\|f(h) + g(r_s) - f(t)\|_2 - \|f(h) + g(r_s) - f(\tilde{t})\|_2 + \Delta] \\
&\quad + \mathbb{E}_{\tilde{h} \sim \mathcal{E} \setminus h} [\|f(h) + g(r_s) - f(t)\|_2 - \|f(\tilde{h}) + g(r_s) - f(t)\|_2 + \Delta] \tag{A.17} \\
&\propto 2\|f(h) - f(t)\|_2 - \mathbb{E}_{\tilde{t} \sim \mathcal{E} \setminus t} \|f(h) - f(\tilde{t})\|_2 - \mathbb{E}_{\tilde{h} \sim \mathcal{E} \setminus h} \|f(\tilde{h}) - f(t)\|_2.
\end{aligned}$$

□

Definition A.4. *Functionally similar molecules.* Assume that $h, t \in \mathcal{E}$ are two molecular entities. h and t are functionally similar if there exists some $o \in \mathcal{E}$ and $r \in \mathcal{R}$ that satisfies: $(h, r, o) \in KG, (t, r, o) \in KG$ or $(o, r, h) \in KG, (o, r, t) \in KG$. We define:

$$\begin{aligned}
\mathcal{I}_1 &= \{(h, r, o), (t, r, o) | (h, r, o) \in KG, (t, r, o) \in KG\}, \\
\mathcal{I}_2 &= \{(o, r, h), (o, r, t) | (o, r, h) \in KG, (o, r, t) \in KG\}, \tag{A.18}
\end{aligned}$$

and $\mathcal{I} = \mathcal{I}_1 \cup \mathcal{I}_2$. We further assume that $|\mathcal{I}| \ll n$, indicating there are not too many intermediate entities connecting h and t , which is common among biomedical knowledge bases.

Lemma A.2. *For functionally similar molecules h and t , the following holds:*

$$\|f(h) - f(t)\| \leq \alpha \mathbb{E}_{(e_1, r, e_2) \sim \mathcal{I}} [\mathcal{L}_{\text{kgc}}(e_1, r, e_2)] + C, \tag{A.19}$$

where $\alpha \approx 1, C \approx 0$ are constants.

Proof. Following [6], we rewrite \mathcal{L}_{kge} as follows based on Eq. A.12 and Eq. A.13:

$$\begin{aligned}\mathcal{L}' &= \mathbb{E}_{(e_1, r, e_2) \sim \mathcal{I}} [\mathcal{L}_{kge}(e_1, r, e_2)] \\ &= \frac{1}{|\mathcal{I}|} \sum_{e_1, e_2 \in \mathcal{E}, r \in \mathcal{R}} \frac{(2N\mathcal{X}_{e_1, r, e_2} - d_{e_1, r}^{out} - d_{e_2, r}^{in})d(e_1, r, e_2)}{N-1} + 2\Delta,\end{aligned}\quad (\text{A.20})$$

where $\mathcal{X}_{e_1, r, e_2} = 1$ indicates $(e_1, r, e_2) \in \mathcal{I}$ and $\mathcal{X}_{e_1, r, e_2} = 0$ indicates $(e_1, r, e_2) \notin \mathcal{I}$. Further, the following inequalities hold:

$$d_{e_1, r}^{out} = \sum_{e_2 \in \mathcal{E}} \mathcal{X}_{e_1, r, e_2} \leq |\mathcal{I}|, d_{e_2, r}^{in} = \sum_{e_1 \in \mathcal{E}} \mathcal{X}_{e_1, r, e_2} \leq |\mathcal{I}|. \quad (\text{A.21})$$

Based on Assumption. 1 we have $d(e_1, r, e_2) \leq \eta + \Delta$ where $\eta = \min_{(e_1, r, e_2) \in KG} [d(e_1, r, e_2)]$, and we assume that $\eta \approx 0$.

Based on Eq. A.20 and Eq. A.21, we have:

$$\begin{aligned}\sum_{(e_1, r, e_2) \in \mathcal{I}} d(e_1, r, e_2) &\leq \frac{1}{2(N-|\mathcal{I}|)} \sum_{(e_1, r, e_2) \in \mathcal{I}} (2N - d_{e_1, r}^{out} - d_{e_2, r}^{in})d(e_1, r, e_2) \\ &= \frac{1}{2(N-|\mathcal{I}|)} \left[|\mathcal{I}|(N-1)(\mathcal{L}' - 2\Delta) + \sum_{(e_1, r, e_2) \notin \mathcal{I}} (d_{e_1, r}^{out} + d_{e_2, r}^{in})d(e_1, r, e_2) \right] \\ &\leq \frac{1}{2(N-|\mathcal{I}|)} [|\mathcal{I}|(N-1)(\mathcal{L}' - 2\Delta) + 2|\mathcal{I}|N(\Delta + \eta)] \\ &= \frac{|\mathcal{I}|(N-1)}{2(N-|\mathcal{I}|)} \mathcal{L}' + \frac{|\mathcal{I}|(N-1)\Delta + |\mathcal{I}|N(\Delta + \eta)}{N-|\mathcal{I}|} \\ &= \frac{|\mathcal{I}|(N-1)}{2(N-|\mathcal{I}|)} \mathcal{L}' + \frac{|\mathcal{I}|(\Delta + N\eta)}{N-|\mathcal{I}|}\end{aligned}\quad (\text{A.22})$$

Then we have:

$$\begin{aligned}\|f(h) - f(t)\| &\leq \min \left\{ \min_{(h, r, o) \in \mathcal{I}_1} \{d(h, r, o) + d(t, r, o)\}, \min_{(o, r, h) \in \mathcal{I}_2} \{d(o, r, h) + d(o, r, t)\} \right\} \\ &\leq \min \left\{ \frac{2}{|\mathcal{I}_1|} \sum_{(e_1, r, e_2) \in \mathcal{I}_1} d(e_1, r, e_2), \frac{2}{|\mathcal{I}_2|} \sum_{(e_1, r, e_2) \in \mathcal{I}_2} d(e_1, r, e_2) \right\} \\ &\leq \frac{2}{|\mathcal{I}|} \sum_{(e_1, r, e_2) \in \mathcal{I}} d(e_1, r, e_2) \\ &\leq \frac{N-1}{N-|\mathcal{I}|} \mathcal{L}' + \frac{2(\Delta + N\eta)}{N-|\mathcal{I}|} \\ &= \alpha \mathcal{L}' + C\end{aligned}\quad (\text{A.23})$$

Since $|\mathcal{I}| \ll N$ and $\eta \approx 0$, we derive that $\alpha \approx 1$ and $C \approx 0$. \square

B Analysis of knowledge graph embedding

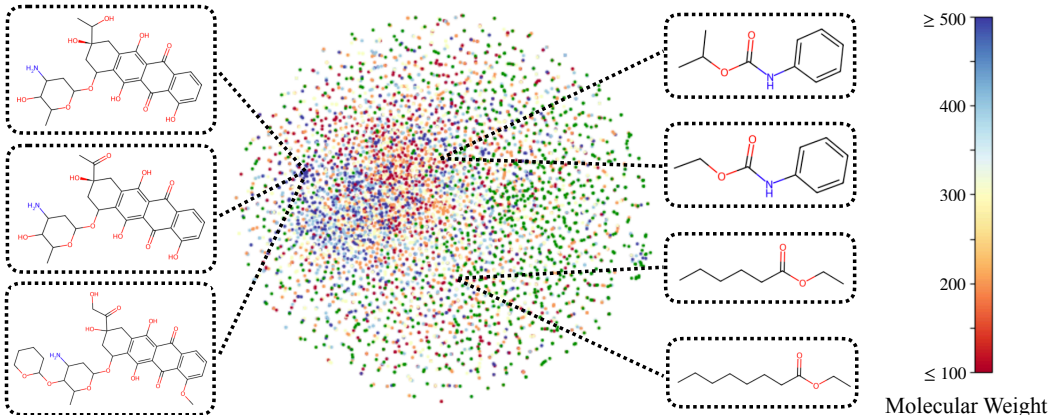


Figure A.1: Visualization of knowledge graph embeddings. Green dots represent entities that are not molecules. Other dots are colored based on molecular weight. We also present molecules that are structurally similar.

Table A.1: Average distance between different molecules

Molecules	structurally similar	functionally similar	random
Avg. distance	1.235	1.287	1.410

In this section, we present additional analysis of knowledge graph embeddings. In Fig. A.1 we illustrate the embeddings of MolFM knowledge encoder for 5,000 randomly sampled entities from the knowledge graph. These embeddings are then visualized using TSNE [8], with molecules being color-coded based on their molecular weights. We also include randomly selected molecules that exhibit similar molecular structures or functions. Notably, Fig. A.1 demonstrates that the learned knowledge features show distinct clustering trends for structurally or functionally similar molecules. For instance, all three molecules on the left of the figure contain 4-amino-5-hydroxy-6-methyloxan-2-yl groups, and their pairwise Morgan fingerprint similarity [9] is no less than 0.78.

Furthermore, we calculate the average distance between structurally similar molecules, functionally similar molecules and random molecules in Tab. A.1. Though the distance between molecules sharing similar structures or functions are not close to 0, they display a significant margin compared to randomly selected molecules. In our experiments, we set a relatively small $\Delta = 0.2$ to stabilize training, and the gradient is clipped to zero if the margin between positive samples and negative samples exceeds Δ , which prohibits further optimization. However, it’s still worth noting that KGE substantially brings structurally or functionally similar molecules closer while pushing dissimilar molecules apart.

C Pre-training dataset and knowledge graph details

We utilize the same molecule-text pairs as introduced by [10]. This dataset contains 15,613 molecules collected from PubChem [11], a comprehensive database of chemical substances and their biological activities as well as 37M paragraphs from S2ORC [12], a versatile corpus for text mining in scientific papers. [10] utilizes simple rules such as using molecular names as queries to obtain molecule-text pairs. Then, we build a knowledge graph for the 15,613 molecules and more with the following steps:

Aligning entities in different databases. The knowledge graph focuses on drugs (molecules), proteins (targets), diseases and other biomedical entities. We collect additional molecules from DrugBank [13], a public database containing structured drug information, and perform duplicate elimination by comparing the isomeric SMILES strings to the 15,613 molecules in our pre-training data. Proteins are identified using Uniprot [14], a widely used protein database. We identify diseases and other entities using MeSH (Medical Subject Headings) [15], a standard vocabulary thesaurus maintained by U.S. National Library of Medicine.

Building connections between entities. The knowledge graph consists of relations including drug-target interaction, drug-drug similarity relationship, drug-drug interaction, and drug-disease association. We build these connections in the following:

For drug-target interactions, we collect drug targets, drug enzymes, drug carriers, and drug transporters from DrugBank. Furthermore, we incorporate BindingDB [16], a public database of biomolecular interactions based on binding affinities. We compare the isomeric SMILES of our molecules with the BindingDB compounds, and extract their protein targets with binding affinity values $K_i \leq 10nM$.

For drug-drug similarity relationships, we leverage MHFP [17], an efficient molecular fingerprint to find k -nearest neighbors from all the molecules in our knowledge graph (we use $k = 10$ in the study). We further compare the RDKit fingerprint similarity [18] between the molecule with the k candidates, and use a threshold of 0.8 to build drug-drug similarity relations. In cases where none of the candidates satisfies the threshold, we further lower the threshold to 0.6 to ensure connectivity.

For drug-drug interactions, we adopt relationships from DrugBank, and further categorize them into 12 classes based on the patterns of their textual description, including *increased activities*, *decreased activities*, *increase risk/severity of adverse effect*, *decrease risk/severity of adverse effect*, *increased metabolism*, *decreased metabolism*, *increase of therapeutic efficacy*, *decrease of therapeutic efficacy*, *increased excretion rate*, *decreased excretion rate*, *increased serum concentration*, *decreased serum concentration*.

For relationships between drugs, diseases and other entities, we collect data from the online platform of FORUM [19], a knowledge base that supports queries for PubChem molecules. We select the most trustworthy associations with $q_value < 10^{-6}$.

The overall statistics of our knowledge graph are presented in Tab. A.2.

Table A.2: Statistics of entities and relations of our knowledge graph. ddi denotes drug-drug interaction.

Entities		ddi: increased metabolism	110,958
molecules	29,043	ddi: decreased metabolism	288,010
diseases	19,655	ddi: increase of therapeutic efficacy	46,492
proteins	403	ddi: decrease of therapeutic efficacy	211,108
All	49,111	ddi: increased excretion rate	56,768
Relations		ddi: decreased excretion rate	390,120
drug-protein interaction	23,870	ddi: increased serum concentration	79,536
ddi: increased activities	294,738	ddi: decreased serum concentration	25,048
ddi: decreased activities	82,712	drug-drug similarity	95,804
ddi: increase risk/severity of adverse effect	1,044,749	drug-disease	499,745
ddi: decrease risk/severity of adverse effect	880	All	3,253,238

D Downstream task details

Here we provide the implementation details for fine-tuning MolFM and other baseline models. For all fine-tuning experiments, we use Adam optimizer with a weight decay of 10^{-5} and select a learning rate from $\{10^{-4}, 3 \times 10^{-4}, 10^{-3}\}$. We run experiments for either 100 or 200 epochs with 3 different random seeds. We employ early-stopping with a patience of 20 epochs.

Cross-modal retrieval. We evaluate our model on the modified PCdes [20] dataset. The original PCdes is collected from PubChem and consists of 15K molecules. We remove 8 molecules whose SMILES strings could not be transformed into a 2D graph by RDKit, and filter out 3,880 molecules that have appeared in our pre-training dataset to prevent information leakage. We adopt Scaffold split [21] instead of random split to evaluate the generalization capability of retrieval models with a train/validation/test ratio of 7:1:2. We conduct both paragraph-level and sentence-level cross-modal retrieval. In paragraph-level retrieval, we use the whole description for the molecule as text input. In sentence-level retrieval, we randomly pick one sentence for each molecule as text input. During fine-tuning, we optimize max of hinge loss between the cosine similarity of structural and textual representations within a minibatch of size 32. For SciBERT [22], KV-PLM [20] and KV-PLM* [20], we use the language model to simultaneously encode 1D SMILES strings and texts. As for the

GraphMVP [23] baseline, we use GraphMVP to encode 2D molecular graphs and employ SciBERT to encode texts.

Molecule captioning. We utilize the ChEBI-20 [24] dataset with 33,010 molecule-description pairs. We follow the original 8:1:1 train/validation/test split. Evaluation metrics include BLEU [25], ROUGE [26], METEOR [27] and Text2Mol score [24]. GraphMVP shares the same architecture as MolFM, where atom features are concatenated with the outputs of the MolT5 [28] encoder. The concatenation result is then fed into the MolT5 decoder to generate molecular descriptions.

Text-based molecule generation. We conduct experiments on ChEBI-20 with the same split as molecule captioning. Evaluation metrics include BLEU, exact ratio (ratio of generated SMILES strings that are identical to the ground truth), valid ratio (ratio of generated SMILES strings that correspond to valid molecules), Levenshtein distance [29], fingerprint Tanimoto similarity (we use MACCS fingerprint [30], Morgan fingerprint [9], RDKit fingerprint [18]) and Text2Mol score. For SciBERT and MoMu, we feed the outputs of the 6th transformer layer into the MolT5 decoder to ensure that they contain the same amount of parameters as MolFM’s text encoder.

Molecular property prediction. We adopt classification datasets in MoleculeNet, a widely used molecular property benchmark. Tab. A.3 provides a summary of the dataset statistics. We follow the same Scaffold split as [23] with a train/validation/test ratio of 8:1:1. To obtain knowledge inputs for each molecule in the dataset, we first compare the isomeric SMILES to molecules in the knowledge graph for an exact match. If there is no exact match, we select a molecule entity in our knowledge graph that has the highest RDKit fingerprint Tanimoto similarity. If the fingerprint similarity is not greater than 0.8, the knowledge input will be a "null" entity with random embeddings. For additional text inputs for each molecule in the dataset, we compare the isomeric SMILES to molecules in ChEBI-20 to find an exact match and obtain the corresponding description. If there is no exact match, the text input will be "No description for the drug is available". During fine-tuning, we perform additional hyper-parameter search on the dropout ratio of MolFM’s structure encoder from {0, 0.1, 0.3, 0.5}.

Table A.3: Summary of molecular property prediction datasets. # Molecules: number of molecules. # Tasks: number of prediction objectives. # Linked to KG: number of molecules that we obtain knowledge graph inputs. # Linked to text: number of molecules that we obtain text inputs.

Dataset	BBBP	Tox21	ToxCast	SIDER	ClinTox	MUV	HIV	BACE
# Molecules	2,039	7,831	8,597	1,427	1,478	93,807	41,127	1,513
# Tasks	1	12	617	27	2	17	1	1
# Linked to KG	1,605	6,328	6,892	1,140	1,151	9,006	8,131	232
# Linked to text	599	2,537	2,538	599	585	219	426	3

E Additional experiments

Tab. A.4 and Tab. A.5 show the paragraph-level cross-modal retrieval results and error bars under fine-tuning setting. Tab. A.7 and Tab. A.6 show the sentence-level cross-modal retrieval results and error bars under zero-shot and fine-tuning settings. Tab. A.8 and Tab. A.2 present the molecule captioning results and error bars. Tab. A.9 and Tab. A.10 display the text-based molecule generation results and error bars.

In addition, we conduct ablation studies on the number of neighbors N . We pre-train MolFM with different choices of N and evaluate the zero-shot paragraph-level cross-modal retrieval performance, as shown in Fig. A.3. We observe that when $N \leq 4$, aggregating information from more neighbors slightly improves the retrieval performance. However, when $N > 4$, increasing N has little impact on our model, which can be attributed to two reasons. Firstly, the sparsity of our knowledge graph results in only a few entities being connected to more than 4 neighbors. Secondly, the interaction relationships between molecules and other entities may exhibit certain patterns or dependencies. Hence, including additional neighbors beyond a certain point may introduce redundant information that does not provide substantial benefits to the representation learning of our model.

Table A.4: Fine-tuned paragraph-level structure-to-text (S-T) retrieval results on the test split of PCdes.

Model	MRR	R@1	R@5	R@10
SciBERT	24.98 \pm 0.88	16.32 \pm 0.92	33.91 \pm 0.88	42.64 \pm 1.88
KV-PLM	27.41 \pm 0.80	18.35 \pm 0.70	37.15 \pm 1.19	45.43 \pm 0.79
KV-PLM*	29.15 \pm 0.47	20.60 \pm 0.53	37.87 \pm 0.65	45.74 \pm 0.56
GraphMVP	31.57 \pm 0.64	23.26 \pm 0.67	40.21 \pm 0.41	47.39 \pm 0.63
MoMu	34.29 \pm 0.69	24.47 \pm 0.64	45.38 \pm 1.25	53.84 \pm 0.83
MolFM	39.56 \pm 0.64	29.76 \pm 0.70	50.53 \pm 0.38	58.63 \pm 0.26

Table A.5: Fine-tuned paragraph-level text-to-structure (T-S) retrieval results on the test split of PCdes.

Model	MRR	R@1	R@5	R@10
SciBERT	23.92 \pm 0.80	14.97 \pm 0.79	34.05 \pm 1.03	41.74 \pm 1.88
KV-PLM	25.97 \pm 1.04	16.55 \pm 1.25	35.85 \pm 1.15	44.75 \pm 0.86
KV-PLM*	28.12 \pm 0.49	19.29 \pm 0.45	37.33 \pm 0.53	45.29 \pm 0.26
GraphMVP	30.93 \pm 0.40	21.94 \pm 0.52	40.28 \pm 0.25	47.90 \pm 0.39
MoMu	34.53 \pm 1.54	24.87 \pm 1.55	44.93 \pm 1.51	54.25 \pm 1.27
MolFM	39.34 \pm 0.70	29.39 \pm 0.81	50.26 \pm 0.65	58.49 \pm 0.98

Table A.6: Sentence-level structure-to-text (S-T) retrieval results on the test split of PCdes.

Mode	Model	MRR	R@1	R@5	R@10
zero-shot	MoMu	5.95	3.05	7.24	10.97
	MolFM	12.54	8.00	16.10	21.23
fine-tune	SciBERT	12.27 \pm 0.27	6.59 \pm 0.21	17.26 \pm 0.27	23.16 \pm 0.41
	KV-PLM	12.93 \pm 0.91	7.15 \pm 1.01	17.84 \pm 0.70	23.88 \pm 0.41
	KV-PLM*	14.59 \pm 0.29	8.64 \pm 0.24	19.98 \pm 0.54	26.22 \pm 0.42
	GraphMVP	14.76 \pm 1.09	8.96 \pm 1.01	19.84 \pm 1.42	25.70 \pm 1.16
	MoMu	19.91 \pm 0.66	12.98 \pm 0.81	26.66 \pm 0.81	33.64 \pm 0.66
	MolFM	21.14 \pm 0.80	14.09 \pm 0.75	28.18 \pm 0.82	35.31 \pm 0.68

Table A.7: Sentence-level text-to-structure (T-S) retrieval results on the test split of PCdes.

Mode	Model	MRR	R@1	R@5	R@10
zero-shot	MoMu	6.18	3.01	7.73	12.37
	MolFM	13.48	8.23	17.76	22.98
fine-tune	SciBERT	11.79 \pm 0.42	6.25 \pm 0.45	16.41 \pm 0.40	22.46 \pm 0.23
	KV-PLM	12.29 \pm 0.83	6.71 \pm 0.83	16.79 \pm 0.88	23.49 \pm 0.28
	KV-PLM*	14.24 \pm 0.26	8.28 \pm 0.15	19.72 \pm 0.30	26.28 \pm 0.42
	GraphMVP	14.75 \pm 1.20	9.04 \pm 1.02	19.73 \pm 1.79	25.60 \pm 1.72
	MoMu	20.10 \pm 1.07	13.23 \pm 1.09	26.81 \pm 1.32	33.76 \pm 1.11
	MolFM	21.54 \pm 0.11	14.49 \pm 0.24	28.46 \pm 0.46	35.82 \pm 0.35

Table A.8: BLEU and ROUGE scores of molecule captioning on the test split of ChEBI-20. †: These results are taken from [28].

Decoder	Encoder	BLEU-2	BLEU-4	ROUGE-1	ROUGE-2	ROUGE-L
MolT5-small	MolT5-small [†]	0.519	0.436	0.620	0.469	0.563
	MoMu	0.532 \pm 0.001	0.445 \pm 0.000	0.621 \pm 0.000	0.469 \pm 0.000	0.564 \pm 0.001
	GraphMVP	0.540 \pm 0.002	0.449 \pm 0.001	0.619 \pm 0.002	0.465 \pm 0.002	0.560 \pm 0.001
	MolFM	0.542 \pm 0.002	0.452 \pm 0.001	0.623 \pm 0.001	0.469 \pm 0.001	0.562 \pm 0.002
MolT5-base	MolT5-base [†]	0.540	0.457	0.634	0.485	0.578
	MoMu	0.549 \pm 0.000	0.462 \pm 0.000	0.630 \pm 0.001	0.479 \pm 0.000	0.575 \pm 0.000
	GraphMVP	0.577 \pm 0.003	0.491 \pm 0.002	0.651 \pm 0.002	0.505 \pm 0.002	0.592 \pm 0.002
	MolFM	0.585 \pm 0.002	0.498 \pm 0.001	0.653 \pm 0.002	0.508 \pm 0.001	0.594 \pm 0.002

Figure A.2: MEATOR and Text2Mol scores of molecule captioning on the test split of ChEBI-20. †: These results are taken from [28].

Decoder	Encoder	METEOR	Text2Mol
MolT5-small	MolT5-small [†]	0.551	0.540
	MoMu	0.557 \pm 0.001	0.543 \pm 0.001
	GraphMVP	0.562 \pm 0.002	0.553 \pm 0.003
	MolFM	0.564 \pm 0.002	0.557 \pm 0.002
MolT5-base	MolT5-base [†]	0.569	0.547
	MoMu	0.576 \pm 0.001	0.558 \pm 0.000
	GraphMVP	0.599 \pm 0.003	0.570 \pm 0.002
	MolFM	0.607 \pm 0.002	0.576 \pm 0.002

Figure A.3: Cross-modal retrieval results with different number of sampled neighbors N .

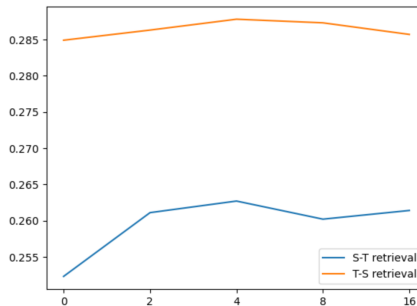


Table A.9: Text-based molecule generation results on the test split of ChEBI-20. †: The higher the better. ‡: The lower the better. †: These results are taken from [28].

Decoder	Encoder	BLEU †	Exact †	Valid †	Levenshtein ‡
MolT5-small	MolT5-small	0.749	0.081	0.724	29.160
	SciBERT	0.797 \pm 0.002	0.142 \pm 0.015	0.846 \pm 0.017	22.027 \pm 0.645
	MoMu	0.800 \pm 0.003	0.150 \pm 0.017	0.858 \pm 0.011	21.446 \pm 0.733
	MolFM	0.803 \pm 0.002	0.169 \pm 0.012	0.859 \pm 0.008	20.868 \pm 0.598
MolT5-base	MolT5-base	0.779	0.082	0.786	25.188
	SciBERT	0.812 \pm 0.002	0.179 \pm 0.011	0.852 \pm 0.014	21.192 \pm 0.612
	MoMu	0.815 \pm 0.002	0.183 \pm 0.014	0.863 \pm 0.014	20.520 \pm 0.757
	MolFM	0.822 \pm 0.002	0.210 \pm 0.013	0.892 \pm 0.012	19.445 \pm 0.745

Table A.10: Text-based molecule generation results on the test split of ChEBI-20. †: The higher the better. ‡: The lower the better. †: These results are taken from [28].

Decoder	Encoder	MACCS FTS †	RDKit FTS †	Morgan FTS †	Text2Mol †
MolT5-small	MolT5-small [†]	0.780	0.653	0.601	0.533
	SciBERT	0.818 \pm 0.005	0.695 \pm 0.009	0.639 \pm 0.016	0.561 \pm 0.007
	MoMu	0.818 \pm 0.007	0.709 \pm 0.010	0.651 \pm 0.009	0.566 \pm 0.004
	MolFM	0.834 \pm 0.006	0.721 \pm 0.008	0.662 \pm 0.011	0.573 \pm 0.004
MolT5-base	MolT5-base [†]	0.787	0.661	0.601	0.543
	SciBERT	0.844 \pm 0.008	0.733 \pm 0.011	0.678 \pm 0.012	0.575 \pm 0.005
	MoMu	0.847 \pm 0.006	0.737 \pm 0.013	0.678 \pm 0.010	0.580 \pm 0.003
	MolFM	0.854 \pm 0.005	0.758 \pm 0.012	0.697 \pm 0.009	0.583 \pm 0.004

F Additional downstream task cases

F.1 Cross-modal retrieval

Fig. A.4 and Fig. A.5 show comparisons between MolFM and MoMu on structure-to-text retrieval and text-to-structure retrieval. We present the structure or text inputs, the top-3 retrieved results for two models, along with the prediction scores and whether the retrieved candidates hit the ground truth.

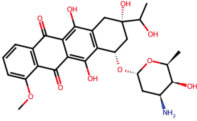
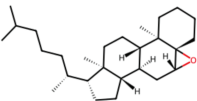
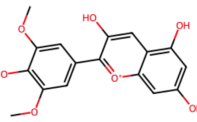
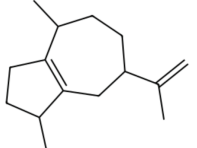
Molecule Input	Model	Top 1	Top 2	Top 3
	MolFM	<p>it is an aminoglycoside antibiotic that is (1S,3S)-3,5,12-trihydroxy-3-(1-hydroxyethyl)-10-methoxy-6,11-dioxo-1,2,3,4,6,11-hexahydro-2,3,6-trideoxy-alpha-L-lyxo-hexopyranosyl residue attached at position 1 via a glycosidic linkage. ...</p> <p>Score: 0.6986 Hit: ✔</p>	<p>it is a sesquiterpene phytoalexin that is (S)-beta-macrocarpene in which the methyl group that is attached to a double bond has undergone formal oxidation to give the corresponding carboxylic acid. It is produced by maize (Zea mays) to provide biochemical protection against fungal... ..</p> <p>Score: 0.6564 Hit: ✗</p>	<p>it is a pyridinecarboxamide that is pyridine-3-carboxamide substituted by a 2,4-difluorophenyl group at the carbamoyl nitrogen and a 3-(trifluoromethyl)phenoxy group at position 2. It has a role as an environmental contaminant, a xenobiotic, a herbicide and a carotenoid biosynthesis inhibitor. ...</p> <p>Score: 0.6200 Hit: ✗</p>
	MoMu	<p>it is a DEA Schedule II controlled substance. Substances in the DEA Schedule II have a high potential for abuse which may lead to severe psychological or physical dependence. ...</p> <p>Score: 0.6220 Hit: ✗</p>	<p>3-Chloro-4-(dichloromethylene)-2,5-pyrrolidinedione belongs to the class of organic compounds known as pyrrolidine-2-ones. These are pyrrolidines which bear a C=O group at position 2 of the pyrrolidine ring. ...</p> <p>Score: 0.5888 Hit: ✗</p>	<p>it is an orally-active benzimidazole derivative with potential anti-neoplastic activity. As a retinoic acid metabolism blocking agent, it inhibits cytochrome P450-dependent all-trans-retinoic acid (ATRA)-4-hydroxylase. ...</p> <p>Score: 0.5739 Hit: ✗</p>
	MolFM	<p>it is the epoxide formed from cholest-5-ene by formal addition of oxygen across the 5,6 double bond with beta-configuration at both C-5 and C-6. It has a role as a mouse metabolite. It derives from a hydride of a 5beta-cholestane. ...</p> <p>Score: 0.7553 Hit: ✔</p>	<p>it is a member of the class of azepinoindoles that is 1,3,4,5-tetrahydro-6H-azepino[5,4,3-cd]indol-6-one carrying additional 4-[(methylamino)methyl]phenyl and fluoro substituents at positions 2 and 8 respectively. ...</p> <p>Score: 0.6907 Hit: ✗</p>	<p>it is a N-sulfonylurea that is N-carbamoyl-3-(ethylsulfonyl)pyridine-2-sulfonamide substituted by a 4,6-dimethoxypyrimidin-2-yl group at the amino nitrogen atom. It has a role as an environmental contaminant, a xenobiotic and a herbicide. ...</p> <p>Score: 0.6743 Hit: ✗</p>
	MoMu	<p>2,5-bis(2-hydroxyethylamino)-3,6-diaziridinylbenzoquinone is a member of the class of 1,4-benzoquinones that is 1,4-benzoquinone in which the hydrogens at positions 2 and 5 have been replaced by aziridin-1-yl groups while the hydrogens at positions 3 and 6 have ...</p> <p>Score: 0.6954 Hit: ✗</p>	<p>1-O-(alpha-D-galactosyl)-N-hexacosanoylphytylphosphingosine is a glycosphingolipid having an alpha-D-galactosyl residue at the O-1 position and a hexacosanoyl group attached to the nitrogen. It has a role as an antineoplastic agent, an epitope, an antigen, an immunological adjuvant and an ...</p> <p>Score: 0.6774 Hit: ✗</p>	<p>it, also known as dihydrojasmonate, belongs to the class of organic compounds known as jasmonic acids. These are lipids containing or derived from a jasmonic acid, with a structure characterized by the presence of an alkene chain linked to a 2-(3-oxocyclopentyl)acetic acid moiety. ...</p> <p>Score: 0.6715 Hit: ✗</p>
	MolFM	<p>it is an anthocyanidin cation that is delphinidin carrying methyl substituents at positions 3' and 5'. It has a role as a biological pigment and a metabolite. It derives from a delphinidin. It is a conjugate acid of a tl(1-). ...</p> <p>Score: 0.6645 Hit: ✔</p>	<p>it is a yellow to light-orange crystalline powder. It has a role as a keratolytic drug, an antineoplastic agent, an antioxidant, a signalling molecule, a retinoid X receptor agonist, an anti-inflammatory agent, an AP-1 antagonist, a it receptor agonist and a human metabolite. ...</p> <p>Score: 0.6083 Hit: ✗</p>	<p>Dimethyl-n-propylamine appears as a colorless liquid. Less dense than water. Contact may irritate skin, eyes and mucous membranes. May be toxic by ingestion. Used to make other chemicals. ...</p> <p>Score: 0.6041 Hit: ✗</p>
	MoMu	<p>it is an aminopyrimidine that is pyrimidin-4-amine substituted by a methyl group at position 2 and a diphosphoxymethyl group at position 5. It has a role as an Escherichia coli metabolite. It is an aminopyrimidine and an alkyl diphosphate. ...</p> <p>Score: 0.6480 Hit: ✗</p>	<p>it is the predominant form of mammalian vasopressin (antidiuretic hormone). It is a nonapeptide containing an arginine at residue 8 and two disulfide-linked cysteines at residues of 1 and 6. ...</p> <p>Score: 0.6154 Hit: ✗</p>	<p>it is a 16-HETE in which the chiral centre at position 16 has S-configuration. It has a role as an anti-inflammatory agent and a human xenobiotic metabolite. It is a conjugate acid of a tl(1-). It is an enantiomer of a 16(R)-HETE. ...</p> <p>Score: 0.6105 Hit: ✗</p>
	MolFM	<p>3, 4-Dihydro-6-methoxy-3, 7-dimethyl-1H-2-benzopyran-8-ol, also known as dhmi-8 or 3, 8-dihydroxy-1, 2, 4-trimethoxyxanthone, belongs to the class of organic compounds known as 2-benzopyrans. These are organic aromatic compounds that 1-benzopyran. ...</p> <p>Score: 0.6558 Hit: ✗</p>	<p>3-Acetyl-1, 2-dithiolane, also known as 1, 2-dithiolane, 3-acetyl, belongs to the class of organic compounds known as 1, 2-dithiolanes. These are organic compounds containing a 1, 2-dithiolane ring. ...</p> <p>Score: 0.6458 Hit: ✗</p>	<p>Alpha-Guaiene, also known as A-guaiene, belongs to the class of organic compounds known as sesquiterpenoids. These are terpenes with three consecutive isoprene units. Alpha-Guaiene is considered to be a practically insoluble (in water) and relatively neutral molecule. ...</p> <p>Score: 0.6439 Hit: ✔</p>
	MoMu	<p>it is a DEA Schedule I controlled substance. Substances in the DEA Schedule I have no currently accepted medical use in the United States, a lack of accepted safety for use under medical supervision, and a high potential for abuse. ...</p> <p>Score: 0.6120 Hit: ✗</p>	<p>it is a dihydroxyflavanone in which the two hydroxy groups are located at positions 5 and 7. A natural product found in Piper sarmentosum and Cryptocarya chartacea. It has a role as an antioxidant, an antineoplastic agent, a vasodilator agent, a neuroprotective agent and a metabolite. ...</p> <p>Score: 0.5960 Hit: ✗</p>	<p>2-Hydroxy-3, 4-dimethoxybenzoic acid belongs to the class of organic compounds known as p-methoxybenzoic acids and derivatives. These are benzoic acids in which the hydrogen atom at position 4 of the benzene ring is replaced by a methoxy group. ...</p> <p>Score: 0.5823 Hit: ✗</p>

Figure A.4: Structure-to-text retrieval examples.

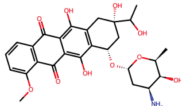
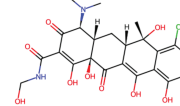
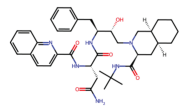
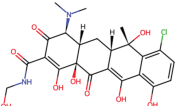
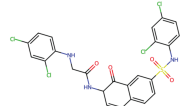
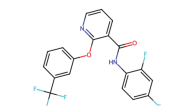
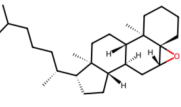
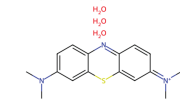
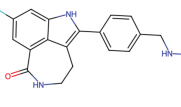
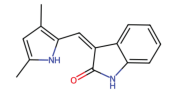
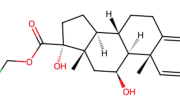
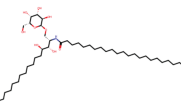
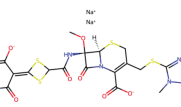
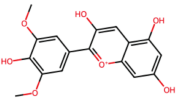
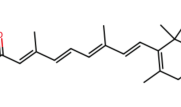
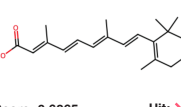
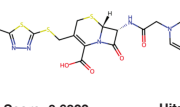
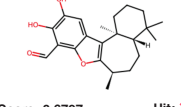
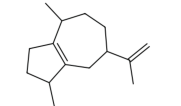
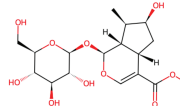
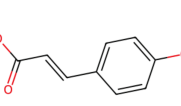
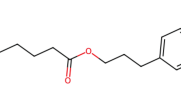
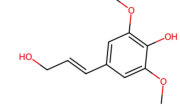
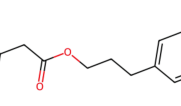
Text Input	Model	Top 1	Top 2	Top 3
<p>it is an aminoglycoside antibiotic that is (1S,3S)-3,5,12-trihydroxy-3-(1-hydroxyethyl)-10-methoxy-6,11-dioxo-1,2,3,4,6,11-hexahydrotetracene having a 3-amino-2,3,6-trideoxy-alpha-L-lyxo-hexopyranosyl residue attached at position 1 via a glycosidic linkage. ...</p>	MolFM	 Score: 0.6986 Hit: ✔	 Score: 0.6500 Hit: ✗	 Score: 0.6087 Hit: ✗
	MoMu	 Score: 0.6954 Hit: ✗	 Score: 0.6774 Hit: ✗	 Score: 0.6715 Hit: ✗
<p>it is the epoxide formed from cholest-5-ene by formal addition of oxygen across the 5,6 double bond with beta-configuration at both C-5 and C-6. It has a role as a mouse metabolite. It derives from a hydride of a 5beta-cholestane.</p>	MolFM	 Score: 0.7553 Hit: ✔	 Score: 0.6884 Hit: ✗	 Score: 0.6734 Hit: ✗
	MoMu	 Score: 0.7407 Hit: ✗	 Score: 0.7069 Hit: ✗	 Score: 0.7061 Hit: ✗
<p>it is an anthocyanidin cation that is delphinidin carrying methyl substituents at positions 3' and 5'. It has a role as a biological pigment and a metabolite. It derives from a delphinidin. It is a conjugate acid of a it(1-).</p>	MolFM	 Score: 0.7264 Hit: ✗	 Score: 0.6645 Hit: ✔	 Score: 0.6168 Hit: ✗
	MoMu	 Score: 0.6865 Hit: ✗	 Score: 0.6822 Hit: ✗	 Score: 0.6797 Hit: ✗
<p>Alpha-Guaiene, also known as A-guaiene, belongs to the class of organic compounds known as sesquiterpenoids. These are terpenes with three consecutive isoprene units. Alpha-Guaiene is considered to be a practically insoluble (in water) and relatively neutral molecule. ...</p>	MolFM	 Score: 0.6439 Hit: ✔	 Score: 0.6290 Hit: ✗	 Score: 0.6052 Hit: ✗
	MoMu	 Score: 0.7821 Hit: ✗	 Score: 0.7805 Hit: ✗	 Score: 0.7312 Hit: ✗

Figure A.5: Text-to-structure retrieval examples.

F.2 Molecule captioning

In Fig. A.6, we illustrate diverse molecules as well as the molecule captioning results of different models. We highlight the text fragments where MolFM generates more accurate expressions that shares similar or exact semantics with the ground truth. However, such contents are missing or incorrect in the outputs of other models.

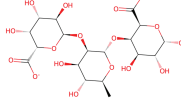
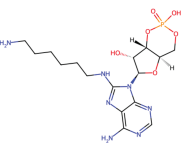
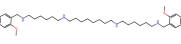
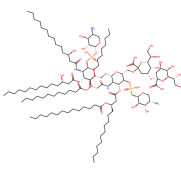
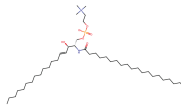
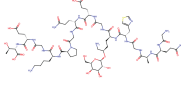
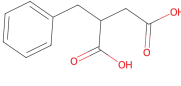
Molecule Input	MolT5 Output	MoMu Output	MolFM Output	Ground Truth
	The molecule is a carbohydrate acid derivative anion obtained by deprotonation of the carboxy groups of alpha-D-Galp, formed by deprotonation of the two carboxy groups. It is the major microspecies at pH 7.3 (according to Marvin v 6.2.0.). It is a carbohy-drate acid derivative anion and a dicarboxylic acid anion. ...	The molecule is a polyanionic polymer obtained by global deprotonation of the carboxy groups of alpha-L-rhamnose. It is a polyanionic polymer and a carbohy-drate acid derivative anion. It is a conjugate base of an al-pha-L-rhamnose.	The molecule is a polyanionic polymer obtained by deprotona-tion of the carboxy groups of [(2R,3S)-4-deoxy-alpha-L-rham-nosyl-(1->4)-alpha-D-galac-turonosyl]-L-iduronic acid; major species at pH 7.3. It is a polyan-ionic polymer and a carbohy-drate acid derivative anion.	The molecule is a polyanionic polymer obtained by deprotona-tion of the carboxy groups of al-pha-D-galacturonosyl-[(1->2)-al-pha-L-rhamnosyl-(1->4)-al-pha-D-galacturonosyl]n; major species at pH 7.3. It is a carbo-hydrate acid anion and a polyanionic polymer.
	The molecule is a 3',5'-cyclic purine nucleotide that is 3',5'-cyclic AMP in which the hy-drogen at position 2 on the purine fragment is replaced by a 6-amino-hexyl group . It is a 3',5'-cyclic purine nucleotide, an adenylyl ribonucleotide, a primary amino compound and a nucleo-tide-sugar. It derives from a 3',5'-cyclic AMP.	The molecule is a 3',5'-cyclic purine nucleotide that is 3',5'-cyclic AMP in which the hydrogen at position 2 on the purine fragment is replaced by a 6-amino-hexyl group . It is a 3',5'-cyclic purine nucleotide, an adenylyl ribonucleotide, a primary amino compound and an aromatic amine. It derives from a 3',5'-cyclic AMP.	The molecule is a 3',5'-cyclic purine nucleotide that is 3',5'-cyclic AMP in which the hydrogen at position 2 on the purine fragment is replaced by a 6-amino-hexylamino group . It is a 3',5'-cyclic purine nucleotide, an adenylyl ribonucleotide, a primary amino compound and an aryl amine. It derives from a 3',5'-cyclic AMP.	The molecule is a 3',5'-cyclic purine nucleotide that is 3',5'-cyclic AMP in which the hydrogen at position 2 on the purine fragment is replaced by a 6-amino-hexylamino group . It is a 3',5'-cyclic purine nucleotide, an adenylyl ribonucleotide, a primary amino compound and a second-ary amino compound. It derives from a 3',5'-cyclic AMP.
	The molecule is a benzamide that is 5-(hexadecyl)hexadecane-1,3-diamine in which one of the amino hydrogens is re-placed by a 7-(3-[4-(2-amino-propyl)amino]butylamino)butyl group. It has a role as an EC 3.1.1.7 (acetylcholinesterase) in-hibitor. It is a member of a ben-zamides, a primary amino com-pound and a primary amino compound.	The molecule is a cyclic ether that is a member of the class of cyclohexa-2,5-dien-1-ylamines in which one of the hydrogens of the amino group is replaced by a benzyl group. It is a cyclic ether and a poly(ethylene glycol).	The molecule is a secondary amino compound that is tetraani-line in which the four amino hy-drogens are replaced by 4-me-thoxyphenyl groups. It has a role as an antileptic drug, a cholin-ergic antagonist and a dopami-nergic antagonist. It is a second-ary amino compound, a tertiary amino compound and an aromatic ether. It derives from a 4-methoxyphenylamine.	The molecule is a tetramine that is N,N'-bis(6-aminoheptyl)oc-tane-1,8-diamine where the pri-mary amino groups both carry 2-methoxybenzyl substituents. It has a role as a muscarinic an-tagonist. It is a tetramine and an aromatic ether. It is a conjugate base of a methoctramine(4+).
Cr	The molecule is a chromium that is cis-cis in which one of the hy-drogens has been replaced by a chromo group. It has a role as a human metabolite, a Saccharo-mycetes cerevisiae metabolite, an Escherichia coli metabolite and a mouse metabolite. It is a chro-mone and a chromone.	The molecule is a chromium co-ordination entity consisting of six chromium cations joined by a double bond. It has a role as a cofactor.	The molecule is a chromium compound that is chromium in which the hydrogen has been re-placed by a Rhdo function. It has a role as a Daphnia magna metabolite and an EC 4.3.1.26 (sterol O-acyltransferase) inhi-bitor. It is a chromium compound and a metal allergen.	The molecule is a chromium group element atom that has atomic number 24. It has a role as a micronutrient. It is a chromi-um group element atom and a metal allergen.
	The molecule is a lipid A deriva-tive having an L-al-pha-D-Hep-(1->5)-[al-pha-D-Kdo-(2->4)]-alpha-Kdo moiety attached to the free primary hydroxy group of lipid A. It is a member of lipid As, a do-decanoate ester and a tetra-decanoate ester. It is a conjugate acid of a heptosyl-(2->6)-al-pha-KDO)2-lipid A(6-).	The molecule is a lipid A deriva-tive having an L-al-pha-D-Hep-(1->5)-[al-pha-D-Kdo-(2->4)]-alpha-Kdo moiety attached to the free primary hydroxy group of lipid A. It is a member of lipid As, a do-decanoate ester and a tetra-decanoate ester. It is a conjugate acid of a heptosyl-(KDO)2-lipid A(6-).	The molecule is a lipid A derivative that consists of a linear tetrasac-charide made up from one L-al-pha-D-Hep-(1->5)-beta-L-arabinopyranosyl residue, two L-glyce-ro-alpha-D-manno-heptose resi-dues (one of which is phosphoeth-anolamine-substituted on O-3), with linkages as shown and with a 3-deoxy-D-manno-oct-2-uloseonic acid (2-keto-3-deoxy-D-mannooct-adeoxy-D-mannopyranosyl group attached. It is a member of lipid As, a tetrasaccharide derivative and a lipid A.	The molecule is a lipid A deriva-tive comprising lipid A glyco-sylated with two 3-deoxy-D-manno-octulosonic acid (KDO) resi-dues and carrying two additional 4-amino-4-deoxy-beta-L-arabinopyranosyl esterifying groups. It is a member of lipid As, a do-decanoate ester and a tetra-decanoate ester. It is a conjugate acid of a (beta-L-Ara4N)2-(K-DO)2-lipid A(2-).
	The molecule is a sphingomyelin d18:1 in which the N-acyl group is specified as docosanoyl It has a role as a mouse metabo-lite. It is a sphingomyelin 40:1 and a sphingomyelin d18:1. It derives from a docosanoic acid.	The molecule is a sphingomyelin d18:1 in which the N-acyl group is specified as icosanoyl It has a role as a mouse metabo-lite. It is a sphingomyelin 40:1 and a sphingomyelin d18:1. It derives from an icosanoic acid.	The molecule is a sphingomyelin d18:1 in which the ceramide N-acyl group is specified as icosanoyl. It has a role as a mouse metabolite. It is a sphingomyelin d18:1 and a sphingomyelin 35:1. It derives from an icosanoic acid.	The molecule is a sphingomyelin d18:1 in which the ceramide N-acyl group is specified as icosanoyl. It has a role as an animal metabolite. It is a sphingomyelin 38:1 and a sphingomyelin d18:1. It derives from an icosanoic acid.
	The molecule is a fifteen-mem-bered glycopeptide comprising glycyl, 3-(1,3-thiazol-4-yl)alanyl , alanyl, glycyl, 3-(1,3-thi-azol-4-yl)alanyl, (5R)-5-(be-ta-D-galactopyranosyloxy)lysyl, glycyl, alpha-glutamyl, gluta-minyl, prolyl, lysyl, glycyl, al-pha-glutamyl and threonine resi-dues coupled in sequence.	The molecule is a fifteen-mem-bered glycopeptide comprising glycyl, homoleucyl , alanyl, glycyl, 3-(1,3-thiazol-4-yl)alanyl, (5R)-5-(beta-D-galactopyranosyloxy)lysyl, glycyl, alpha-glu-tamyl, glutamyl, glycyl, prolyl, lysyl, glycyl, alpha-glutamyl and threonine residues coupled in sequence.	The molecule is a fifteen-mem-bered glycopeptide comprising glycyl, glutamyl , alanyl, glycyl, 3-(1,3-thiazol-4-yl)alanyl, (5R)-5-(beta-D-galactopyranosy-loxy)lysyl, glycyl, alpha-glutamyl, glutamyl, glycyl, prolyl, lysyl, glycyl, alpha-glutamyl and thre-onine residues coupled in se-quence.	The molecule is a fifteen-mem-bered glycopeptide comprising glycyl, glutamyl , alanyl, glycyl, 3-(1,3-thiazol-4-yl)alanyl, (5R)-5-(beta-D-galactopyranosy-loxy)lysyl, glycyl, alpha-glutamyl, glutamyl, glycyl, prolyl, lysyl, glycyl, alpha-glutamyl and thre-onine residues coupled in se-quence.
	The molecule is a phenylalanine derivative that is phenylalaninate in which one of the meta- hydro-gens is substituted by a 3-hy-droxylphenyl group. It is a phe-nylalanine derivative, a member of benzenes and a member of phenols. It derives from a phe-nylalanine and a phenylalanine.	The molecule is a beta-diketone that is malonic acid in which one of the methyl hydrogens is sub-stituted by a phenyl group. It has a role as a metabolite. It de-rives from a malonic acid.	The molecule is a dicarboxylic acid that is glutaric acid in which one of the methyl hydrogens is substituted by a carboxylic acid group. It has a role as a metabo-lite. It derives from a glutaric acid. It is a conjugate acid of a 3-(carboxylatophenyl)-3-phenyl-butanoate.	The molecule is a dicarboxylic acid consisting of succinic acid carrying a 2-benzyl substituent. It has a role as a bacterial xeno-biotic metabolite. It derives from a succinic acid. It is a conjugate acid of a 2-benzylsuccinate(2-) and a (R)-2-benzylsuccinate.

Figure A.6: Additional molecule captioning examples.

E.3 Text-to-molecule generation

Fig. A.7 shows text-to-molecule generation results of different models. We also calculate Morgan fingerprint Tanimoto similarity between the generated molecules and the ground truth.

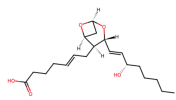
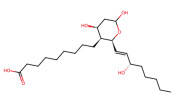
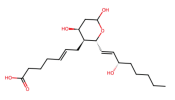
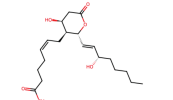
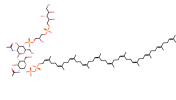
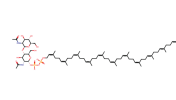
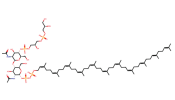
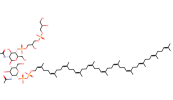
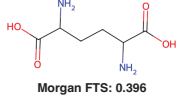
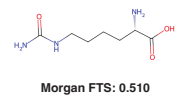
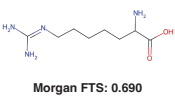
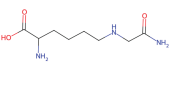
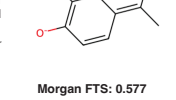
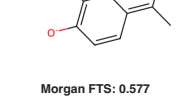
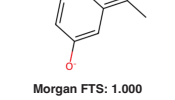
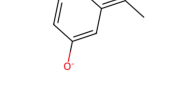
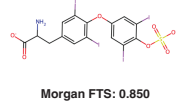
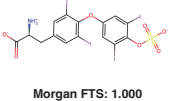
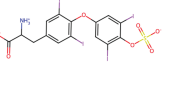
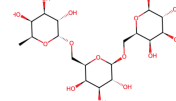
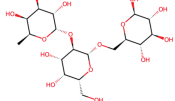
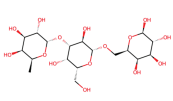
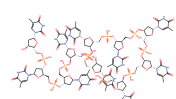
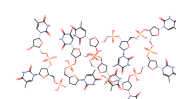
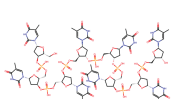
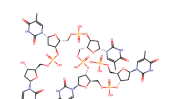
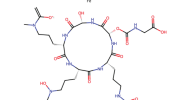
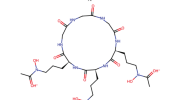
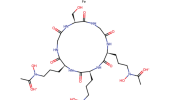
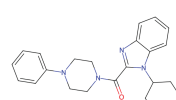
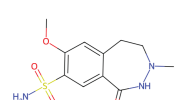
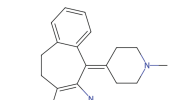
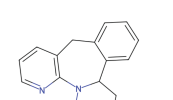
Molecule Input	MolT5 Output	MoMu Output	MolFM Output	Ground Truth
<p>The molecule is a thromboxane obtained by formal oxidation of the hemiacetal hydroxy function of thromboxane B2. It has a role as a human metabolite. It derives from a thromboxane B2. It is a conjugate acid of an 11-dehydro-thromboxane B2(1-).</p>				
	Morgan FTS: 0.670	Morgan FTS: 0.485	Morgan FTS: 0.735	
<p>The molecule is a linear tetrasaccharide derivative consisting of beta-D-galactose, alpha-D-galactose, beta-L-rhamnose and beta-D-glucose residues linked sequentially (1->2), (1->3) and (1->4), with the glucose residue linked glycosidically to a 5-aminopentyl group. It is a tetrasaccharide derivative and a glycoside.</p>				
	Morgan FTS: 0.942	Morgan FTS: 0.809	Morgan FTS: 1.000	
<p>The molecule is a lysine derivative in which the N(epsilon) of the amino acid carries a carbamoylmethyl group. It is a lysine derivative and a non-proteinogenic alpha-amino acid.</p>				
	Morgan FTS: 0.396	Morgan FTS: 0.510	Morgan FTS: 0.690	
<p>The molecule is a steroid ester that is methyl (17E)-pregna-4,17-dien-21-oate substituted by oxo groups at positions 3 and 11. It is a 3-oxo-Delta(4) steroid, an 11-oxo steroid, a steroid ester and a methyl ester. It derives from a hydride of a pregnane.</p>				
	Morgan FTS: 0.577	Morgan FTS: 0.577	Morgan FTS: 1.000	
<p>The molecule is conjugate base of thyroxine sulfate having anionic carboxy and sulfate groups and the amino group protonated. It is a 3,3',5-triiodo-L-thyronine and a phenyl sulfate oxoanion. It is a conjugate base of a thyroxine sulfate.</p>	Invalid			
	Morgan FTS: 0.000	Morgan FTS: 0.850	Morgan FTS: 1.000	
<p>The molecule is a trisaccharide consisting of alpha-L-fucopyranose and two beta-D-galactopyranose residues joined in sequence by (1->3) and (1->6) glycosidic bonds. It derives from a beta-(1->6)-galactobiose and an alpha-L-fucose.</p>	Invalid			
	Morgan FTS: 0.000	Morgan FTS: 0.778	Morgan FTS: 0.913	
<p>The molecule is an oligonucleotide comprising five deoxythymidic acid residues linked 5'->3'. It contains a thymidine 5'-monophosphate residue, a dTMP 5'-end residue and a dTMP 3'-end residue.</p>				
	Morgan FTS: 0.500	Morgan FTS: 0.500	Morgan FTS: 0.629	
<p>The molecule is a member of the class of ferrichromes that is an iron(III) chelate of the homodetic cyclic hexapeptide cyclo(glycyl-L-seryl-glycyl-N(5)-acetyl-N(5)-hydroxy-L-ornithyl-N(5)-acetyl-N(5)-hydroxy-L-ornithyl-N(5)-acetyl-N(5)-hydroxy-L-ornithyl). It has a role as a metabolite.</p>	Invalid			
	Morgan FTS: 0.000	Morgan FTS: 0.432	Morgan FTS: 0.840	
<p>The molecule is a benzazepine and a tetracyclic antidepressant. It has a role as an alpha-adrenergic antagonist, a serotonergic antagonist, a histamine antagonist, an anxiolytic drug, a H1-receptor antagonist and a oneirogen.</p>				
	Morgan FTS: 0.250	Morgan FTS: 0.134	Morgan FTS: 0.441	

Figure A.7: Additional text-to-molecule generation cases. "Invalid" indicates that the generated SMILES can not be converted to a 2D molecular graph.

G Additional visualization of cross-modal attention

Fig. A.8 shows the normalized cross-modal attention from texts to atoms. Fig. A.9 shows the normalized cross-modal attention from texts to neighbors in the knowledge graph.

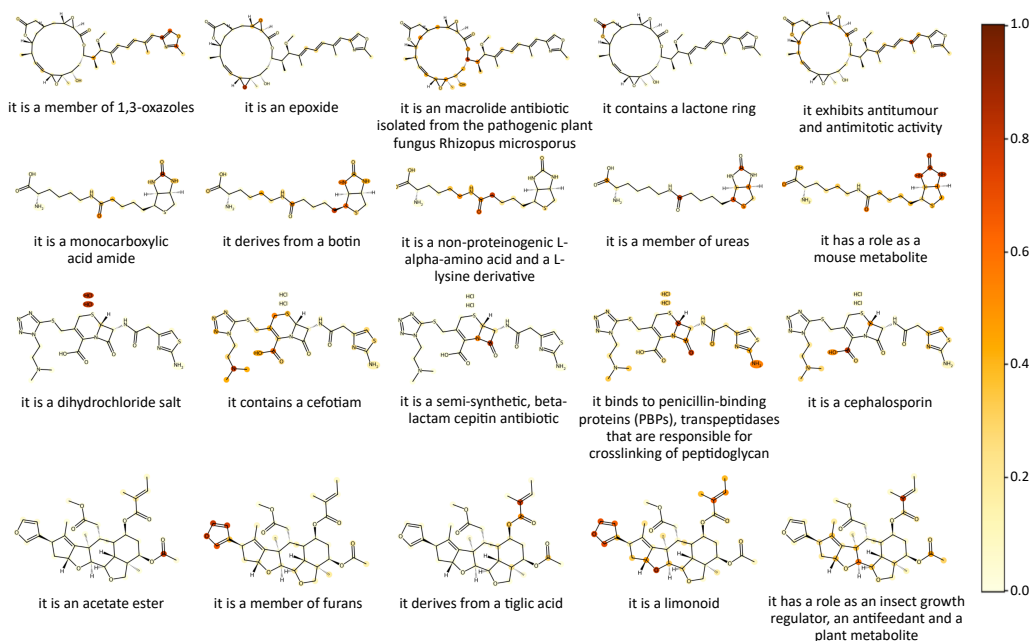


Figure A.8: Additional visualization of cross-modal attention from texts to atoms.

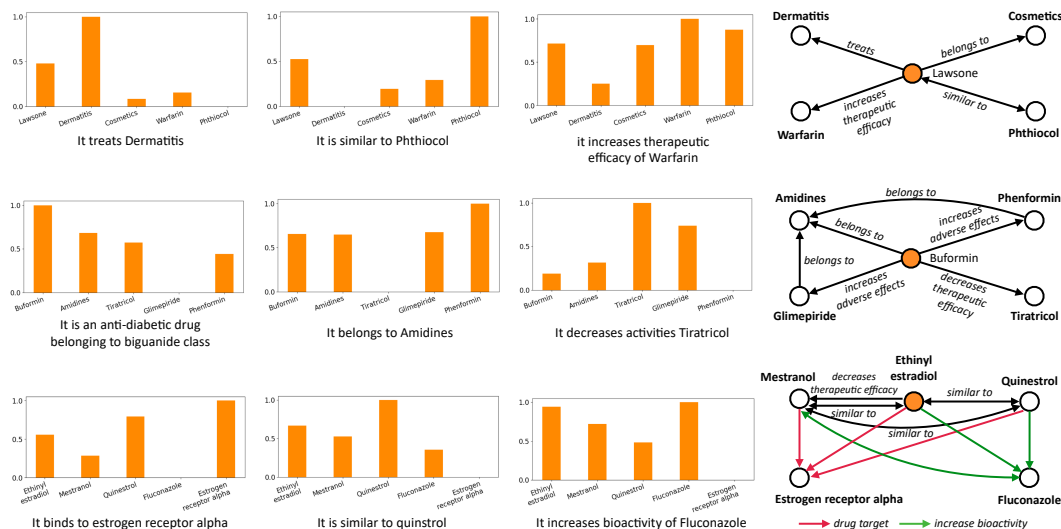


Figure A.9: Additional visualization of cross-modal attention from texts to neighbors. **Left:** the input text and the normalized attention to each entity. **Right:** the selected molecule (orange) and 4 randomly sampled neighboring entities, as well as relationships between these entities.

Appendix

- [1] Elad Hoffer and Nir Ailon. Deep metric learning using triplet network. In *Similarity-Based Pattern Recognition: Third International Workshop, SIMBAD 2015, Copenhagen, Denmark, October 12-14, 2015. Proceedings 3*, pages 84–92. Springer, 2015.
- [2] Mahmut Kaya and Hasan Şakir Bilge. Deep metric learning: A survey. *Symmetry*, 11(9):1066, 2019.
- [3] Aaron van den Oord, Yazhe Li, and Oriol Vinyals. Representation learning with contrastive predictive coding. *arXiv preprint arXiv:1807.03748*, 2018.
- [4] Junnan Li, Ramprasaath Selvaraju, Akhilesh Gotmare, Shafiq Joty, Caiming Xiong, and Steven Chu Hong Hoi. Align before fuse: Vision and language representation learning with momentum distillation. *Advances in neural information processing systems*, 34:9694–9705, 2021.
- [5] Mengying Sun, Jing Xing, Huijun Wang, Bin Chen, and Jiayu Zhou. Mocl: Data-driven molecular fingerprint via knowledge-aware contrastive learning from molecular graph. In *Proceedings of the 27th ACM SIGKDD Conference on Knowledge Discovery & Data Mining*, pages 3585–3594, 2021.
- [6] Jiezhong Qiu, Hao Ma, Yuxiao Dong, Kuansan Wang, and Jie Tang. Revisiting knowledge base embedding as tensor decomposition. 2018.
- [7] Antoine Bordes, Xavier Glorot, Jason Weston, and Yoshua Bengio. A semantic matching energy function for learning with multi-relational data: Application to word-sense disambiguation. *Machine Learning*, 94:233–259, 2014.
- [8] Laurens Van der Maaten and Geoffrey Hinton. Visualizing data using t-sne. *Journal of machine learning research*, 9(11), 2008.
- [9] David Rogers and Mathew Hahn. Extended-connectivity fingerprints. *Journal of chemical information and modeling*, 50(5):742–754, 2010.
- [10] Bing Su, Dazhao Du, Zhao Yang, Yujie Zhou, Jiangmeng Li, Anyi Rao, Hao Sun, Zhiwu Lu, and Ji-Rong Wen. A molecular multimodal foundation model associating molecule graphs with natural language. *arXiv preprint arXiv:2209.05481*, 2022.
- [11] Sunghwan Kim, Paul A Thiessen, Evan E Bolton, Jie Chen, Gang Fu, Asta Gindulyte, Lianyi Han, Jane He, Siqian He, Benjamin A Shoemaker, et al. Pubchem substance and compound databases. *Nucleic acids research*, 44(D1):D1202–D1213, 2016.
- [12] Kyle Lo, Lucy Lu Wang, Mark Neumann, Rodney Kinney, and Daniel S Weld. S2orc: The semantic scholar open research corpus. In *Proceedings of the 58th Annual Meeting of the Association for Computational Linguistics*, pages 4969–4983, 2020.
- [13] David S Wishart, Yannick D Feunang, An C Guo, Elvis J Lo, Ana Marcu, Jason R Grant, Tanvir Sajed, Daniel Johnson, Carin Li, Zinat Sayeeda, et al. Drugbank 5.0: a major update to the drugbank database for 2018. *Nucleic acids research*, 46(D1):D1074–D1082, 2018.
- [14] UniProt Consortium. Uniprot: a worldwide hub of protein knowledge. *Nucleic acids research*, 47(D1):D506–D515, 2019.
- [15] Carolyn E Lipscomb. Medical subject headings (mesh). *Bulletin of the Medical Library Association*, 88(3):265, 2000.
- [16] Michael K Gilson, Tiqing Liu, Michael Baitaluk, George Nicola, Linda Hwang, and Jenny Chong. Bindingdb in 2015: a public database for medicinal chemistry, computational chemistry and systems pharmacology. *Nucleic acids research*, 44(D1):D1045–D1053, 2016.
- [17] Daniel Probst and Jean-Louis Reymond. A probabilistic molecular fingerprint for big data settings. *Journal of cheminformatics*, 10:1–12, 2018.

- [18] Nadine Schneider, Roger A Sayle, and Gregory A Landrum. Get your atoms in order—an open-source implementation of a novel and robust molecular canonicalization algorithm. *Journal of chemical information and modeling*, 55(10):2111–2120, 2015.
- [19] Maxime Delmas, Olivier Filangi, Nils Paulhe, Florence Vinson, Christophe Duperier, William Garrier, Paul-Emeric Saunier, Yoann Pitarch, Fabien Jourdan, Franck Giacomoni, et al. building a knowledge graph from public databases and scientific literature to extract associations between chemicals and diseases. *Bioinformatics*, 37(21):3896–3904, 2021.
- [20] Zheni Zeng, Yuan Yao, Zhiyuan Liu, and Maosong Sun. A deep-learning system bridging molecule structure and biomedical text with comprehension comparable to human professionals. *Nature communications*, 13(1):862, 2022.
- [21] Guy W Bemis and Mark A Murcko. The properties of known drugs. 1. molecular frameworks. *Journal of medicinal chemistry*, 39(15):2887–2893, 1996.
- [22] Iz Beltagy, Kyle Lo, and Arman Cohan. Scibert: A pretrained language model for scientific text. In *Proceedings of the 2019 Conference on Empirical Methods in Natural Language Processing and the 9th International Joint Conference on Natural Language Processing (EMNLP-IJCNLP)*, pages 3615–3620, 2019.
- [23] Shengchao Liu, Hanchen Wang, Weiyang Liu, Joan Lasenby, Hongyu Guo, and Jian Tang. Pre-training molecular graph representation with 3d geometry. In *ICLR 2022 Workshop on Geometrical and Topological Representation Learning*, 2022.
- [24] Carl Edwards, ChengXiang Zhai, and Heng Ji. Text2mol: Cross-modal molecule retrieval with natural language queries. In *Proceedings of the 2021 Conference on Empirical Methods in Natural Language Processing*, pages 595–607, 2021.
- [25] Kishore Papineni, Salim Roukos, Todd Ward, and Wei-Jing Zhu. Bleu: a method for automatic evaluation of machine translation. In *Proceedings of the 40th annual meeting of the Association for Computational Linguistics*, pages 311–318, 2002.
- [26] Chin-Yew Lin. Rouge: A package for automatic evaluation of summaries. In *Text summarization branches out*, pages 74–81, 2004.
- [27] Satanjeev Banerjee and Alon Lavie. Meteor: An automatic metric for mt evaluation with improved correlation with human judgments. In *Proceedings of the acl workshop on intrinsic and extrinsic evaluation measures for machine translation and/or summarization*, pages 65–72, 2005.
- [28] Carl Edwards, Tuan Lai, Kevin Ros, Garrett Honke, and Heng Ji. Translation between molecules and natural language. *arXiv preprint arXiv:2204.11817*, 2022.
- [29] Frederic P Miller, Agnes F Vandome, and John McBrewster. *Advanced encryption standard*. Alpha Press, 2009.
- [30] Joseph L Durant, Burton A Leland, Douglas R Henry, and James G Nourse. Reoptimization of mdl keys for use in drug discovery. *Journal of chemical information and computer sciences*, 42(6):1273–1280, 2002.